NATIONAL ADVISORY COMMITTEE FOR AERONAUTICS

TECHNICAL NOTE 3651

CROSS FLOWS IN LAMINAR INCOMPRESSIBLE BOUNDARY LAYERS

By Arthur G. Hansen and Howard Z. Herzig

Lewis Flight Propulsion Laboratory
Cleveland, Ohio

Washington
February 1956

NATIONAL ADVISORY COMMITTEE FOR AERONAUTICS

TECHNICAL NOTE 3651

CROSS FLOWS IN LAMINAR INCOMPRESSIBLE BOUNDARY LAYERS

By Arthur G. Hansen and Howard Z. Herzig

SUMMARY

An analysis is derived for the three-dimensional boundary-layer flow over a flat surface with a leading edge under main-flow streamlines which are translates and representable by polynomial expressions. The boundary layers are laminar and incompressible, and the profiles of their velocity components have similarity with respect to rectangular coordinates. Solutions are obtained for main-flow streamlines representable by polynomials up to the 11^{th} order. Flow-visualization experimental checks for the theory are provided for several flow configurations and for comparisons of the behavior of thick and thin boundary layers.

INTRODUCTION

Many useful applications of the theory for laminar two-dimensional boundary-layer flow have been made for estimating losses in turbomachines for design purposes. However, substantial portions of these losses are known to derive from the effects of three-dimensional turbulent-boundary-layer behavior. Secondary flows in turbomachines (herein defined as boundary-layer flows having components normal to the mainstream flows, which result from mainstream turning, and from radial force and pressure gradients), for example, give rise to boundary-layer accumulations and significant losses in the blade end regions. These secondary-flow phenomena cannot be explained by extensions of the two-dimensional boundary-layer theory. Consequently, the importance of understanding the three-dimensional turbulent-boundary-layer behavior has led to many experimental and theoretical investigations in recent years. The experimental investigations of secondary flows (refs. 1 to 3) have proved useful in interpreting and correlating flow measurements taken in turbomachines under actual operating conditions. Furthermore, the results indicate that laminar-boundary-layer behavior can usefully provide qualitative information concerning turbulent-boundary-layer behavior.

From a theoretical viewpoint, the importance of the practical applicability of laminar-boundary-layer flow studies cannot be exaggerated.

Turbomachine boundary layers are quite generally turbulent. Theoretical three-dimensional boundary-layer investigations, however, are largely confined to laminar-flow studies, because the nonlinear partial-differential equations involved, while formidable for the laminar case, are practically unsolvable for the turbulent case. Thus, it is fortunate that the results of laminar investigations qualitatively retain practical significance for turbomachine research.

A well-known secondary-flow manifestation is the cross-channel flow of the end-wall boundary layers in turbomachines (refs. 1 to 3) due to the pressure gradients developed by the mainstream turning. In these references, the cross-channel-flow streamlines approach a limiting position at the wall. This cannot be accounted for by nonviscous-flow theories. Consequently, the more complicated viscous boundary-layer theory must be employed for these secondary flows. References 4 to 7 analyze the laminar-boundary-layer cross flow developments over a surface having a leading edge. In references 5 and 6 exact solutions are obtained for cases of main streamlines consisting of parabolic-shaped translates (i.e., the entire streamline pattern can be obtained by translating a parabolic-shaped streamline in a direction parallel to the leading edge) with no restrictions on the turning. In references 4 and 7 approximate solutions are obtained for more general main streamline shapes, restricted to regions of small turning.

Likewise assuming laminar main streamline translates, this report extends these analyses and obtains exact solutions for general streamline paths without restrictions to regions of small turning. Tables of special functions of the Blasius similarity parameter required for computing such boundary-layer crossflows are presented. It is shown that some of the results of the small perturbation analysis of reference 7 need not be restricted to regions of small turning. The streamline paths at various positions in the boundary layer are presented for thick and thin boundary layers. Certain interesting examples of cross-channel flows are computed. For some of these, cross-channel effects are observed experimentally by means of smoke-flow-visualization procedures and compared with the theoretical predictions.

This work was done at the NACA Lewis laboratory during the summer of 1955.

ANALYSIS

The equations for determining the steady incompressible laminar-boundary-layer flow over a surface with coordinate axes oriented as in figure 1 are

$$u\frac{\partial u}{\partial x} + v\frac{\partial u}{\partial y} + w\frac{\partial u}{\partial z} - \nu\frac{\partial^2 u}{\partial y^2} = X - \frac{1}{\rho}\frac{\partial p}{\partial x} \tag{1a}$$

$$u\frac{\partial w}{\partial x} + v\frac{\partial w}{\partial y} + w\frac{\partial w}{\partial z} - \nu\frac{\partial^2 w}{\partial y^2} = Z - \frac{1}{\rho}\frac{\partial p}{\partial z} \tag{1b}$$

$$\frac{\partial u}{\partial x} + \frac{\partial v}{\partial y} + \frac{\partial w}{\partial z} = 0 \text{ (continuity eq.)} \tag{1c}$$

(All symbols are defined in appendix A.) The boundary conditions for the system of equations are

$$u = v = w = 0 \qquad \text{for } y = 0$$

$$\lim_{y\to\infty} u = U$$

$$\lim_{y\to\infty} w = W$$

The present investigation is concerned with two-dimensional mainstream flows, which exhibit no variation in velocity components in the z-direction. Such flows are characterized by the fact that their sreamlines form a system of "translates." That is, the entire streamline pattern can be obtained by translating any particular streamline parallel to the leading edge of the surface (fig. 2). This uniformity of flow will be reflected in the boundary-layer behavior, and it follows that the boundary-layer velocities will likewise have no variation in the z-direction. Using these facts and expressing the right side of equations (1a) and (1b) in terms of the mainstream velocity components result in

$$u\frac{\partial u}{\partial x} + v\frac{\partial u}{\partial y} - \nu\frac{\partial^2 u}{\partial y^2} = U\frac{\partial U}{\partial x} \tag{2a}$$

$$u\frac{\partial w}{\partial x} + v\frac{\partial w}{\partial y} - \nu\frac{\partial^2 w}{\partial y^2} = U\frac{\partial W}{\partial x} \tag{2b}$$

$$\frac{\partial u}{\partial x} + \frac{\partial v}{\partial y} = 0 \tag{2c}$$

From the general class of mainstream flows described, solutions are obtained for $W = W_i$ in equations (2a) and (2b) for mainstream flows defined by equations (3) and (4),

$$U = U_0 \text{ (a constant)} \tag{3}$$

$$W_i = a_i x^i \tag{4}$$

The condition $U = U_0$ is considered a reasonable approximation for most turbomachine configurations. An exact solution, however, for $W = ax$ is presented in references 5 and 6. Substitution of equations (3) and (4) into (2a) and (2b) yields

$$u\frac{\partial u}{\partial x} + v\frac{\partial u}{\partial y} - \nu\frac{\partial^2 u}{\partial y^2} = 0 \tag{5a}$$

$$u\frac{\partial w}{\partial x} + v\frac{\partial w}{\partial y} - \nu\frac{\partial^2 w}{\partial y^2} = U_0 i a_i x^{i-1} \tag{5b}$$

Examination of equations (5a) and (2c) and the boundary conditions reveals that these equations are identical to the boundary-layer equations for flow over a flat surface in a uniform stream. The solution of these equations is the well-known Blasius solution

$$u = U_0 F'(\eta) \tag{6}$$

$$v = \frac{1}{2}\sqrt{\frac{\nu U_0}{x}}\,(\eta F' - F) \tag{7}$$

where

$$\eta = y\sqrt{\frac{U_0}{\nu x}} \tag{8}$$

and F is the Blasius function (tabulated in table I).

In equation (6) the crossflow boundary-layer velocity component in the x-direction is expressed as a function of the parameter η. The boundary-layer velocity component in the z-direction can be expressed similarly. Thus, the function $P_i(\eta)$ is sought such that

$$w = W_i P_i(\eta) \tag{9}$$

Substituting equations (6), (7), and (9) into (5b) and simplifying yield

$$P_i'' + \frac{FP_i'}{2} - iF'P_i + i = 0 \tag{10}$$

The boundary conditions are

$$P_i(0) = 0$$

$$\lim_{\eta \to \infty} P_i(\eta) = 1$$

Equation (10) is a total-differential equation for the function $P_i(\eta)$. As F and F' are known in tabulated form (table I), a solution for $P_i(\eta)$ may be obtained through application of numerical analysis (appendix B). The values of the $P_i(\eta)$ and $P_i'(\eta)$ functions (i = 1 to 10) are tabulated in table II. Values of $P_i(\eta)$ are plotted in figure 3(a). It should be noted that $P_0(\eta)$ equals $F'(\eta)$.

The preceding results can be generalized at once. Assume that the mainstream velocity component W is given by

$$W = \sum_{i=0}^{m} W_i \tag{11}$$

where

$$W_i = a_i x^i$$

It may be verified by substitution that if w_i denotes that solution of equation (5b) as expressed by equation (9), then $w = \sum_{i=0}^{m} w_i = \sum_{i=0}^{m} W_i P_i$ along with equations (6) and (7) constitutes the solution of equations (2) for the mainstream flow defined by equations (3) and (11). Thus for $U = U_0$, a solution for the boundary-layer flow can be obtained for any main streamline shape which can be reasonably approximated by a polynomial.

Results similar to those given can be deduced from the analysis presented in reference 7. However, this particular analysis is of the small-perturbation type and assumes small total turning of the mainstream flow (i.e., $W << U_0$). It can be seen now that this restriction is unnecessary.

Main-Flow Streamlines

The streamlines of the main flow can be obtained from the relation between streamline slope and velocity components

$$\frac{dz}{dx} = \frac{W}{U_0} = \frac{\sum_{i=0}^{m} a_i x^i}{U_0} \tag{12}$$

From equation (12),

$$z = \text{constant} + a_0^* x + \frac{a_1^* x^2}{2} + \ldots + \frac{a_m^* x^{m+1}}{m+1} \tag{13}$$

where

$$a_i^* = \frac{a_i}{U_0}$$

As the coefficients in equation (13) are arbitrary, a variety of streamline shapes can be constructed by the proper choice of a_i^*. A particular shape (e.g., the contour of a channel wall) may be approximated by constructing an approximating polynomial according to usual numerical procedures. In this respect, the class of flows becomes a useful tool in investigating the influence of various streamline configurations on boundary-layer behavior.

Boundary-Layer Streamlines

The projection of a boundary-layer streamline in a plane normal to the leading edge of the surface (i.e., parallel to the x,y-plane) may be obtained from the relation along the streamline

$$\frac{dy}{dx} = \frac{v}{u} = \frac{\frac{1}{2}\sqrt{\frac{\nu U_0}{x}}}{U_0 F'} (\eta F' - F) \tag{14}$$

Along a streamline y is a function of x; hence along a streamline η is a function of x only. By differentiating $\eta = y\sqrt{\frac{U_0}{\nu x}}$ and combining with equation (14) to eliminate dy/dx, there results a simple total-differential equation

$$\frac{dx}{x} = -2\frac{F'}{F} d\eta \tag{15}$$

Thus, along a given streamline in the boundary layer,

$$x = \frac{K}{[F(\eta)]^2} \tag{16}$$

By specifying the initial values x_0 and η_0, $F(\eta_0)$ can be obtained from table I, and the value of the constant stream function K can be calculated. For this value of K, $F(\eta)$ hence η and $P_i(\eta)$ can be obtained from the tables for all values of x along the streamline.

With a correspondence established between x and η for all points along the streamline, y can be computed from $y = \eta\sqrt{\frac{\nu x}{U_0}}$. Thus, the projection of the streamline in the x,y-plane, normal to the surface, is easily obtained from the tables.

The projection of a boundary-layer streamline in a plane parallel to the surface can be obtained from the relation

$$\frac{dz}{dx} = \frac{w}{u} = \sum_{i=0}^{m} \frac{W_i P_i(\eta)}{U_0 F'} = \sum_{i=0}^{m} a_i^* x^i J_i(\eta) \tag{17}$$

where

$$J_i = \frac{P_i}{F'}$$

The values of $J_i(\eta)$ are tabulated in table III. With a correspondence established between x and η along a streamline by equation (16), the right side of equation (17) is expressible as a function of x alone; and it follows that

$$z = \sum_{i=0}^{m} \int_{x_0}^{x} a_i^* x^i J_i(\eta)\,dx + z_0 \tag{18}$$

Numerical integration of equation (18) will then yield the shape of the streamline projection in the plane parallel to the surface. The actual three-dimensional boundary-layer streamline paths are then determined from a combination of the two projected views. The boundary-layer velocity components u, v, and w are computed directly from equations (6), (7), and (9).

In experimental studies of three-dimensional boundary flows over flat surfaces, it is evident that the boundary-layer streamlines near the surface approach a limiting shape (ref. 2). Theoretical determination of this "limiting streamline" is possible for the present problem by evaluating equation (17) at $y = 0$. This yields

$$\frac{dz}{dx} = \sum_{i=0}^{m} a_i^* x^i J_i(0) \tag{19}$$

Therefore, by direct integration of equation (19), the following equation of the limiting streamlines (dependent only on the geometry of the mainstream flow) results

$$z_{\eta=0} = \sum_{i=0}^{m} \frac{a_i^* x^{(i+1)}}{i+1} J_i(0) + z_0 \tag{20}$$

The value $J_i(0) = \frac{P_i(0)}{F'(0)} = \frac{0}{0}$ can be determined by use of L'Hospital's rule

$$\lim_{\eta \to 0} \frac{P_i(\eta)}{F'(\eta)} = \frac{P_i'(0)}{F''(0)}$$

The $P_i'(0)$ values are obtained (see table II) during the numerical solutions of equation (10). The quantity $F''(0)$ is 0.33206 (ref. 8).

By inspection of equation (20), the shape of the limiting-deflection boundary-layer streamline is seen independent of the inlet velocity U_0. The other boundary-layer streamlines are functions of η (eq. (18)) and thus are not independent of U_0.

Normal and Tangential Velocity Components

In order to obtain a better physical picture of boundary-layer flow in relation to mainstream flow, it is often desirable to resolve boundary-layer velocities into components tangent and normal to the mainstream flow direction. Denoting the tangential component by t and the normal component by n, it can be shown (appendix C) that

$$\frac{n}{U_0} = n^* = \frac{1}{T} \sum_{i=0}^{m} W_i^* H_i \tag{21}$$

$$\frac{t}{U_0} = t^* = F'T^* + W^* n^* \tag{22}$$

where

$$T \equiv \sqrt{U_0^2 + W^2}$$

$$H_i = P_i - F'$$

and * denotes division by U_0. The function H is tabulated in table IV and plotted in figure 3(b).

RESULTS AND DISCUSSION

Calculation of Functions

Solutions of equation (10) for various values of i have been presented in several publications. References 5 and 6 present solutions for i = 1 with a tabular listing of the functional values given in the latter reference. Reference 7 contains solutions for i = 0, 1, 2, 3, 4, and -1/2 in graphical form. In the present report, negative values of the exponent i have not been investigated, because they require infinite velocities at the leading edge of the surface. Where i = 0, $P_0 \equiv F'$.

In the present investigation, solutions of equation (10) were obtained for integral values of i ranging from 0 to 10. The results (values of $P_i(\eta)$ and $P_i'(\eta)$) are presented in tabular form (table II) and $P_i(\eta)$ in graphical form (fig. 3). A description of the method for numerical solutions of equation (10) is provided in appendix B.

Flow With Circular-Arc Streamlines

As an application of the theory, the boundary-layer development for a flow with circular-arc streamlines was investigated. The specific flow region analyzed is restricted to that shown in figure 4. As seen in the figure, the flow is normal to the leading edge of the surface and crosses the downstream boundary of the region at 45°.

Polynomial approximation. - The equation of the family of circular arcs depicted in figure 4 is

$$z = c - (1 - x^2)^{1/2} \tag{23}$$

where c is an arbitrary constant, and $0 \leqq x \leqq \frac{\sqrt{2}}{2}$. By series expansion, equation (23) is expressible as

$$z = c - 1 + \frac{x^2}{2} + \frac{x^4}{8} + \frac{x^6}{16} + \ldots$$

$$= z_0 + \frac{x^2}{2} + \frac{x^4}{8} + \frac{x^6}{16} + \ldots \tag{24}$$

where $z_0 \equiv c - 1$. By selecting the first four terms of equation (24), the polynomial

$$z = z_0 + \frac{x^2}{2} + \frac{x^4}{8} + \frac{x^6}{16} \tag{25}$$

is obtained. This polynomial then serves as an approximation to the streamlines of the main flow and is used to apply the theory to the determination of the boundary-layer characteristics.

Boundary-layer streamlines. - Streamlines in the boundary layer are obtained from simultaneous solution of equations (16) and (18) previously described. In the present example, three representative streamlines were computed beginning at the position $x = 0.05$, and at positions corresponding, respectively, to 1/4, 1/2, and 3/4 of the boundary-layer thickness. The initial value of x was chosen at 0.05 instead of at the surface leading edge because of the singularity in the flow equations at $x = 0$. From table II and figure 3 it is seen that a value of η which reasonably defines the "outer edge" of the boundary layer is 6.4. Accordingly, the values $\eta = 1.6$, 3.2, and 4.8 respectively correspond to positions at 1/4, 1/2, and 3/4 of the boundary-layer thickness.

A plot of these streamlines including the limiting boundary-layer streamline determined from equation (20) is given in figure 5. These streamline paths are similar in form to the boundary-layer overturning on the end walls of the circular-arc sheet-metal cascades (as visualized and presented in ref. 1) before passage vortex roll-up occurs.

Velocity profiles. - The profiles of the velocity components n^* and t^* at $x = 0.2$, 0.4, and 0.6 are presented in figure 6. It is interesting to note that the n^* profiles have maximum values for $\eta < 1.3$, that is, in the lower fifth of the boundary layer. An examination of the curves for H_i (fig. 3(b)) and equation (21) indicates that, in general, if the coefficients in the polynomial approximation of the flow streamlines $W_i^* = a_i^* x^i$ are positive, then n^* will always have a maximum value for $\eta < 1.3$ (cf. ref. 4). This can be directly associated with the discussion on vorticities of the cross-channel boundary-layer flow in blade rows (ref. 3). In this reference, the cross-channel "double" boundary-layer flow is considered as divided into two regions.

In the region near the wall, n^* rises from zero at the wall to some maximum value in the sublayer of the boundary layer. In the upper boundary-layer region, n^* declines from this maximum value to zero at the mainstream. These two distributions of velocity may be associated with vorticities of opposite signs in the two parts of the boundary layer. It is further hypothesized that such vorticities generate the actual flow vortices observed in blade passages (ref. 3). However, visualization studies in various blade passages generally indicate only simple passage-flow vortices. Usually there is either no evidence at all of the formation of a flow vortex from boundary-layer crossflow in the sublayer adjacent to the wall or at best a formation that is small and poorly defined. It is therefore conjectured that the narrowness of the boundary-layer sublayer and the large viscous forces in that region tend to prevent the sizable roll-up characteristic of vortex formation in the upper boundary-layer region. The position of the maximum value of n^* in figure 6 and the shape of the H_i curves (fig. 3(b)) both substantiate this conjecture.

Overturning in Thick and Thin Boundary Layers for 60° Bends

In a theoretical and experimental investigation, a comparison was made between the overturning of a relatively thick and a thin boundary layer for 60° mainstream turning.

Theoretical comparisons of overturning. - A theoretical comparison of thick- and thin-boundary-layer overturning was made by determining the overturning of the boundary layer near the surface for two mainstream flows (consisting of streamline translates described by eq. (13)).

The flow field whose main-flow streamlines are represented in the thick-boundary-layer case by

$$z = \frac{k^*}{6} x^6 + z_0 \qquad 0 \leq x \leq 1 \tag{26}$$

is shown in figure 7. The value k^* is taken equal to $\sqrt{3}$ for 60° mainstream turning. The boundary-layer development in the long nearly straight inlet section provides a thick boundary layer at $x = 0.5$, the region where appreciable turning begins.

In the thin-boundary-layer case, with streamlines represented by

$$z = \frac{k^*}{6} (x + 0.5)^6 + z_0 \qquad 0 \leq x \leq 0.5 \tag{27}$$

in figure 8, the appreciable turning begins right at the leading edge with no chance for prior boundary-layer build-up. The turning sections for the two cases are identical. The boundary-layer streamlines are presented in figures 9 and 10.

The thicker boundary layer (figs. 7 and 9) overturns more rapidly than the thinner boundary layer (figs. 8 and 10). Physically, it would be expected that thicker boundary layers with lower viscous shear forces would have sharper cross-channel overturning than thinner boundary layers with correspondingly higher viscous shear forces. The theoretical results agree with expectations. Comparable results were obtained in experiments (ref. 3) in turbine nozzle blade configurations. The results of reference 2 demonstrate the larger response of thicker turbine blade boundary layers to radial pressure gradients than thin blade boundary layers. The fundamental question remains as to whether or not the theory presented herein has any immediate demonstrable application to actual flow behavior other than in a purely general sense. This problem was investigated experimentally by means of flow visualization.

Experimental comparison of overturning. - The main flow, which is a system of streamline translates, can be considered as the flow through a two-dimensional cascade of a large number of very thin blades having the main streamline shape with vanishingly small blade spacing. As in axisymmetric flow theories, the blades supply the required force field (eqs. (1)) for the prescribed flow turning. For such channels with very small spacing, the turning is very close to the streamline-translates turning. Thus, an ideal one-dimensional analysis indicates that, on the basis of continuity and turning considerations, the flow velocities should approximate the theoretical translate flow velocities quite closely.

An experimental investigation was made to determine if the theory provides a reasonable approximation to the boundary-layer overturning in a channel with spacing more nearly comparable to that found in turbomachine configurations. The experimental determination and comparison of thick- and thin-boundary-layer overturning was made by means of smoke-flow visualization (apparatus and procedures described in ref. 1) in two-dimensional rectangular bends with channel shapes the same as the previously described main streamlines.

With a maximum Reynolds number of about 6×10^4, the flow for these tests was well within the laminar range. Figure 11 shows the mainstream-flow paths traced by means of smoke. As expected, boundary-layer accumulations near the suction surface cause the mainstream to deviate somewhat from the desired streamline shape. Nevertheless, by keeping the solidity of the turning section high (approx. 2.0), sufficient mainstream guidance is provided to maintain the mean streamline close to the desired shape.

The overturning of the end-wall boundary layers as visualized by means of smoke for both the thick and thin boundary layers is shown in figures 12(a) and (b), respectively. The smoke was introduced through static taps at the inlet to the turning sections of the bends. Because of the obvious difficulties in accurately locating streamlines at various heights within the boundary layer, attention was devoted mainly to obtaining the limiting line ($\eta = 0$) of the flow along the end wall. The experimental cross-channel limiting deflection (fig. 12) corresponds closely to the theoretical predictions, except near the region of boundary-layer accumulation at the suction surface.

Because the smoke traces always appear faint in overhead photographic shots (see ref. 1), the pictures of the thin boundary layer presented in figure 13 were taken looking upstream and can be compared with a simultaneous overhead photograph. The photographs indicate that, in the region near the wall, the theory predicts overturning very satisfactorily.

Boundary-layer velocity profiles. - The velocity profiles of n^* and t^* for the thick and the thin boundary layers are presented in figures 14 and 15, respectively. The values are plotted at equally spaced intervals of x within the turning sections of the bends and at corresponding locations (i.e., at $x = 0.5, 0.6, 0.7, 0.8, 0.9$, and 1.0 for the thick-boundary-layer case and at $x = 0.1, 0.2, 0.3, 0.4$, and 0.5 for the thin-boundary-layer case). The n^* and the t^* profiles peak at lower η values for the thick than for the thin boundary layer. For the thick boundary layer (fig. 14), n^* becomes larger than 1 at stations far from the leading edge ($x = 0.9$ and 1.0), indicating that the component of the boundary velocity normal to the mainstream-flow direction has become larger than the inlet velocity U_0. For both thick and thin boundary layers (a sizable portion of the boundary layer), the tangential component t^* at sufficiently large x actually becomes greater than the local mainstream velocity. This is illustrated by the t^* profiles which overshoot and then approach the mainstream T^* values from above.

This theoretical result, likewise observed in reference 5, may be explained as follows: For flows such as are considered herein

$$W = \sum_{i=0}^{m} a_i x^i$$

it can be seen from equation (1b) and by substitution of W_i into equation (2b) to obtain

$$Z - \frac{1}{\rho}\frac{\partial p}{\partial z} = U_0 i \sum_{i=0}^{m} a_i x^{i-1}$$

that there is a gradient of the external force field and the static pressure in the z-direction. With U_0 constant everywhere along the leading edge, there then exists a total-pressure and energy variation along the leading edge. By convection, the more-than-mainstream turning (overturning) of the boundary layer transports boundary-layer material from a region of high total energy into regions of lower mainstream total energy. For sufficient overturning and large enough energy gradients at the inlet, it is possible for regions to exist in which the boundary layer has a higher total energy than the local mainstream does. Because the boundary layer is assumed to have the same static pressure as the mainstream, the boundary-layer velocities must exceed the local mainstream velocities, as illustrated in figure 14. For flows with main streamline translates where the boundary-layer velocity exceeds the local mainstream velocity at some axial distance x from the leading edge, the boundary-layer velocities exceed the local mainstream velocities everywhere downstream of that axial location.

CONCLUDING REMARKS

Experimental verification of boundary-layer overturning for flows in a bend was obtained in this investigation for the laminar-boundary-layer behavior as predicted by a theory based on similarity considerations and main streamline translates. A main streamline through the bend conforms quite closely to the desired flow path. Actually with the great range of possible flow paths describable by an 11^{th} degree polynomial, the requirement of main streamline translates (corresponding to the assumption of axial symmetry in turbomachine design) is not very restrictive. The close agreement obtained between theoretical and experimental boundary-layer overturning indicates that the theoretical assumptions can be considered to be reasonable for this laminar-cross-channel-flow theory. In addition, experimental investigations similarly conducted on other configurations very much like these have provided qualitatively correct information concerning the turbulent-boundary-layer (overturning) behavior for flows at operational speeds in turbomachine configurations. These results indicate that the laminar-boundary-layer theory may provide qualitative information concerning turbulent-boundary-layer behavior.

It is interesting to note that while the theoretical development is based on boundary-layer velocity-profile similarity in the x- and z-directions, the velocity profiles in the z-direction are similar only for a flow described by

$$U = U_0 \tag{3}$$

$$W_i = a_i x^i \tag{4}$$

For a flow in which

$$W = \sum_{i=0}^{m} a_i x^i$$

the profiles of the boundary-layer velocity component, while congruent in the z-direction, are different for every x:

$$w = \sum_{i=0}^{m} w_i = \sum_{i=0}^{m} W_i P_i = \sum_{i=0}^{m} a_i x^i P_i$$

For the flows considered in this report, the profiles of the boundary-layer velocity components in the x-direction are all similar and are related by the Blasius function

$$u = U_0 F'(\eta) \tag{6}$$

and, thus, are identical to the profiles obtained for straight laminar flow over a flat plate.

Lewis Flight Propulsion Laboratory
National Advisory Committee for Aeronautics
Cleveland, Ohio, November 10, 1955

APPENDIX A

SYMBOLS

a, a_i constants, coefficients of polynomials in powers of x

C_1, C_2 constants, trial values chosen for $P_i'(0)$ in numerical solutions

c constant

$F, F(\eta)$ Blasius function (table I)

$H, H_i(\eta)$ function of η, $H_i(\eta) = P_i(\eta) - F'(\eta)$ (table IV)

i constant, $i = 0, 1, 2, \ldots m$

$J, J_i(\eta)$ function of η, $J_i(\eta) = \frac{P_i(\eta)}{F'(\eta)}$ (table III)

K constant of integration for stream equation in x,y-plane

k constant

m constant

n component of boundary-layer velocity normal to mainstream-flow direction

$P, P_i(\eta)$ function of η, $w = \sum_{i=0}^{m} W_i P_i(\eta)$

p static pressure

S, S_1, S_2 indicated solution to related single-point boundary value problem (appendix D)

T $\sqrt{U^2 + W^2}$

t component of boundary-layer velocity tangential to mainstream-flow direction

U, W mainstream velocity components in x- and z-directions, respectively

U_0 inlet velocity

u,v,w boundary velocity components in the x-, y-, and z-directions, respectively

X,Z components of external force field in x- and z-directions, respectively

x,y,z rectangular coordinates

z_0 constant

η similarity variable, $\eta = y\sqrt{\frac{U_0}{\nu x}}$

ν coefficient of kinematic viscosity

ρ density

Subscripts:

i variable index, $i = 0, 1, 2, \ldots m$

m constant

Superscripts:

i variable exponent, $i = 0, 1, 2, \ldots m$

m constant

$'$ differentiation with respect to η

$''$ differentiation with respect to η

$*$ denotes division by U_0

APPENDIX B

CALCULATION OF FUNCTIONS

A linear second-order ordinary differential equation for $P_i(\eta)$

$$P_i'' + \frac{FP_i'}{2} - iF'P_i + i = 0 \tag{10}$$

together with the boundary conditions

$$P_i(0) = 0$$

$$\lim_{\eta \to \infty} P_i(\eta) = 1$$

constitutes a two-point boundary value problem, which may be solved numerically by a method of repeated trials. This is essentially equivalent to considering the system as two related single-point problems with boundary conditions

$$P_i(0) = 0$$

$$P_i'(0) = C_1, C_2$$

where C_1 and C_2 are chosen constants.

With given C_1 and C_2, solutions S_1 and S_2 are obtained, as will be described later in this section, and values are determined for $P_i(\eta)$ at the outer edge of the boundary layer. Because equation (10) is a linear differential equation, linear combinations of S_1 and S_2 can be made based on the values of $P_i(\eta)$ obtained for η large and the boundary condition

$$\lim_{\eta \to \infty} P_i(\eta) = 1$$

Thus,

$$S = kS_1 + (1 - k)S_2$$

where k is the appropriate constant, satisfies the differential equation and the boundary conditions at all points. Because of errors in rounding off, choosing

$$P_i'(0) = kC_1 + (1 - k)C_2$$

will not in general be a boundary condition which will give a satisfactory solution, that is,

$$P_i(\infty) = 1$$

Thus, further interpolations and trials may be required. In the present problem for $i = 1, 2, 3, 4$, a fourth trial was required; for higher values of i, fifth and sixth trials were required.

The numerical integration procedures carried on an IBM Card-Programmed Electronic Calculator consist of two phases (as described in ref. 9), the starting phase and the extension phase. Briefly, in the starting phase, a modified Picard's iteration method is used for the calculation of the first four points, $\eta = 0.05$, 0.10, 0.15, and 0.20. With these as starting values, successive $P_i(\eta)$ values are computed by forward integration. The forward integration is continued until the values of $P_i(\eta)$ become very large, positive or negative, and thus diverge markedly from the required boundary condition

$$\lim_{\eta \to \infty} P_i(\eta) = 1$$

In conformity with the findings of references 5, 7, and 8, $\eta = 8$ was chosen as the outer edge of the boundary layer, and so the outer-boundary condition

$$\lim_{\eta \to \infty} P_i(\eta) = 1$$

becomes

$$P_i(8) = 1$$

The linear interpolations could then be based on the values of $P_i(8)$ obtained by integration. The physical requirement that the boundary layer merge smoothly into the main flow is equivalent to requiring $P_i'(8)$ to equal 0. Therefore, linear interpolation of the values of $P_i'(8)$ obtained in the trial solutions may also be used to provide trial values of $P_i'(0)$.

These functions change rapidly in the range $0 \leq \eta \leq 3.0$ (fig. 3(a)). Consequently, in this range the forward integration was carried out numerically for intervals of $\eta = 0.05$ to ensure sufficient accuracy. For values of η greater than 3.0, the numerical integrations

were made for intervals of $\eta = 0.10$. The values of $P_i(\eta)$ ($i = 1$ to 10) are presented in table II. The suitability of this forward integration process was judged by comparing computations for $P_0 = F'$ with values obtained in established references (e.g., ref. 9). The values were found to check to the five decimal places presented by those references. For convenience, the values of F' are presented in table I for the same intervals as the P functions.

APPENDIX C

RESOLUTION OF BOUNDARY-LAYER VELOCITIES INTO COMPONENTS NORMAL AND TANGENTIAL TO MAIN-FLOW STREAMLINES

Let $z = f(x)$ be the equation of a streamline in the x,z-plane. Then, from figure 16

$$\tan \theta = \frac{dz}{dx} = \frac{W}{U_0} = W^* \tag{C1}$$

$$\cos \theta = \frac{1}{\sqrt{1 + \left(\frac{dz}{dx}\right)^2}} = \frac{1}{\sqrt{1 + \left(\frac{W}{U_0}\right)^2}} = \frac{1}{T^*} \tag{C2}$$

where

$$T = \sqrt{U_0^2 + W^2}$$

$$\sin \theta = \tan \theta \cos \theta = \frac{W^*}{T^*} \tag{C3}$$

The boundary-layer velocity components t and n are obtained from the components u and w by means of the relations (see fig. 16)

$$t = u \cos \theta + w \sin \theta \tag{C4}$$

$$n = w \cos \theta - u \sin \theta \tag{C5}$$

Substitution of equations (C2) and (C3) into (C4) and (C5) yields

$$t = \frac{u}{T^*} + \frac{wW^*}{T^*} = \frac{u + wW^*}{T^*} \tag{C6}$$

$$n = \frac{w - uW^*}{T^*} \tag{C7}$$

Now equation (C7) can be written as

$$n^* = \frac{w^* - u^*W^*}{T^*} = \frac{1}{T^*}\left(\sum_{i=0}^{m} a_i^* x^i P_i - F' \sum_{i=0}^{m} a_i^* x^i\right)$$

$$= \frac{1}{T^*}\sum_{i=0}^{m} a_i^* x^i (P_i - F') = \frac{1}{T^*}\sum_{i=0}^{m} W_i^* H_i \tag{C8}$$

where

$$W_i^* = a_i^* x^i$$

and

$$H_i = P_i - F'$$

Equation (C6) can be expressed as

$$t^* = \frac{u^* + w^* W^*}{T^*} = \frac{F' + W^* \sum_{i=0}^{m} W_i^* P_i}{T^*} \tag{C9}$$

Substitution of $H_i + F'$ for P_i in equation (C9) yields

$$t^* = \frac{F'(1 + W^*)^2 + W^* \sum_{i=0}^{m} W_i^* H_i}{T^*} = \frac{F'(T^*)^2 + W^* \sum_{i=0}^{m} W_i^* H_i}{T^*} \tag{C10}$$

Finally, substituting equation (C8) into (C10) gives

$$t^* = F'T^* + W^* n^* \tag{C11}$$

REFERENCES

1. Herzig, Howard Z., Hansen, Arthur G., and Costello, George R.: A Visualization Study of Secondary Flows in Cascades. NACA Rep. 1163, 1954. (Supersedes NACA TN 2947.)

2. Rohlik, Harold E., Kofskey, Milton G., Allen, Hubert W., and Herzig, Howard Z.: Secondary Flows and Boundary-Layer Accumulations in Turbine Nozzles. NACA Rep. 1168, 1954. (Supersedes NACA TN's 2871, 2909, and 2989.)

3. Kofskey, Milton G., and Allen, Hubert W.: Smoke Study of Nozzle Secondary Flows in a Low-Speed Turbine. NACA TN 3260, 1954.

4. Mager, Artur, and Hansen, Arthur G.: Laminar Boundary Layer over a Flat Plate in a Flow Having Circular Streamlines. NACA TN 2658, 1952.

5. Loos, Henk G.: A Simple Laminar Boundary Layer with Secondary Flow. Jour. Aero. Sci., vol. 22, no. 1, Jan. 1955, pp. 35-40.

6. Sowerby, L.: Secondary Flow in a Boundary Layer. Rep. No. AERO. 2512, British R.A.E., Mar. 1954.

7. Mager, Artur: Three-Dimensional Laminar Boundary Layer with Small Cross-Flow. Jour. Aero. Sci., vol. 21, no. 12, Dec. 1954, pp. 835-845.

8. Schlichting, H.: Lecture Series "Boundary Layer Theory." Pt. I - Laminar Flows. NACA TM 1217, 1949. (Trans. of Vortragsreihe, W.S. 1941/42, LFA Hermann Goring, Braunschweig.)

9. Ostrach, Simon: An Analysis of Laminar Free-Convection Flow and Heat Transfer About a Flat Plate Parallel to the Direction of the Generating Body Force. NACA Rep. 1111, 1953. (Supersedes NACA TN 2635.)

TABLE I. - VALUES OF F AND F'

η	F'	F	η	F'	F	η	F'	F
0	0	0	2.00	0.62977	0.65003	4.90	0.98981	3.18422
.05	.01660	.00042	2.05	.64300	.68185	5.00	.99154	3.28329
.10	.03321	.00166	2.10	.65600	.71432	5.10	.99301	3.38252
.15	.04981	.00374	2.15	.66877	.74744	5.20	.99425	3.48188
.20	.06641	.00664	2.20	.68131	.78120	5.30	.99529	3.58136
.25	.08300	.01038	2.25	.69361	.81557	5.40	.99616	3.68093
.30	.09960	.01494	2.30	.70565	.85055	5.50	.99688	3.78059
.35	.11619	.02034	2.35	.71745	.88613	5.60	.99748	3.88031
.40	.13276	.02656	2.40	.72898	.92229	5.70	.99797	3.98007
.45	.14933	.03361	2.45	.74026	.95903	5.80	.99838	4.07990
.50	.16589	.04149	2.50	.75126	.99632	5.90	.99871	4.17975
.55	.18242	.05020	2.55	.76200	1.03415	6.00	.99897	4.27964
.60	.19894	.05973	2.60	.77246	1.07251	6.10	.99919	4.37955
.65	.21543	.07009	2.65	.78264	1.11139	6.20	.99936	4.47947
.70	.23189	.08128	2.70	.79254	1.15077	6.30	.99950	4.57942
.75	.24832	.09328	2.75	.80217	1.19064	6.40	.99961	4.67937
.80	.26471	.10611	2.80	.81151	1.23098	6.50	.99970	4.77933
.85	.28106	.11975	2.85	.82057	1.27179	6.60	.99977	4.87931
.90	.29735	.13421	2.90	.82934	1.31304	6.70	.99982	4.97929
.95	.31360	.14949	2.95	.83784	1.35472	6.80	.99986	5.07928
1.00	.32978	.16557	3.00	.84605	1.39682	6.90	.99990	5.17927
1.05	.34590	.18246	3.10	.86162	1.48221	7.00	.99992	5.27926
1.10	.36194	.20016	3.20	.87608	1.56910	7.10	.99994	5.37925
1.15	.37790	.21866	3.30	.88945	1.65739	7.20	.99996	5.47925
1.20	.39378	.23795	3.40	.90176	1.74696	7.30	.99997	5.57924
1.25	.40956	.25803	3.50	.91304	1.83771	7.40	.99998	5.67924
1.30	.42524	.27890	3.60	.92333	1.92953	7.50	.99998	5.77924
1.35	.44081	.30056	3.70	.93267	2.02234	7.60	.99999	5.87924
1.40	.45626	.32298	3.80	.94112	2.11604	7.70	.99999	5.97924
1.45	.47159	.34618	3.90	.94872	2.21053	7.80	.99999	6.07924
1.50	.48679	.37014	4.00	.95552	2.30576	7.90	.99999	6.17923
1.55	.50185	.39486	4.10	.96158	2.40162	8.00	1.00000	6.27923
1.60	.51676	.42032	4.20	.96696	2.49805	8.10	1.00000	6.37923
1.65	.53151	.44653	4.30	.97170	2.59499	8.20	1.00000	6.47923
1.70	.54610	.47347	4.40	.97587	2.69237	8.30	1.00000	6.57923
1.75	.56052	.50114	4.50	.97951	2.79015	8.40	1.00000	6.67923
1.80	.57476	.52952	4.60	.98268	2.88826	8.50	1.00000	6.77923
1.85	.58881	.55861	4.70	.98543	2.98667	8.60	1.00000	6.87923
1.90	.60267	.58840	4.80	.98779	3.08533	8.70	1.00000	6.97923
1.95	.61632	.61887				8.80	1.00000	7.07923

TABLE II. - VALUES OF P_1 AND P_1'

η	P_1	P_2	P_3	P_4	P_5	P_6	P_7	P_8	P_9	P_{10}	P_1'	P_2'	P_3'	P_4'	P_5'	P_6'	P_7'	P_8'	P_9'	P_{10}'
0	0	0	0	0	0	0	0	0	0	0	1.4180286	2.1971141	2.8579975	3.4501246	3.99534467	4.50568286	4.98863616	5.4492713	5.8912136+	6.3171697-
.05	.070	.107	.139	.168	.193	.218	.241	.262	.283	.303	1.368	2.097	2.708	3.250	3.746	4.206	4.639	5.050	5.442	5.818
.10	.137	.210	.271	.325	.375	.421	.464	.505	.544	.582	1.318	1.998	2.559	3.051	3.497	3.908	4.292	4.654	4.997	5.324
.15	.201	.307	.395	.473	.543	.609	.670	.728	.783	.836	1.268	1.898	2.411	2.855	3.252	3.615	3.950	4.264	4.559	4.838
.20	.264	.400	.512	.611	.700	.782	.859	.932	1.000	1.066	1.219	1.800	2.264	2.611	3.011	3.326	3.615	3.883	4.132	4.365
.25	.323	.487	.622	.739	.844	.941	1.032	1.116	1.197	1.273	1.170	1.703	2.120	2.470	2.725	3.045	3.290	3.513	3.718	3.908
.30	.381	.570	.724	.858	.977	1.087	1.188	1.283	1.372	1.457	1.121	1.608	1.979	2.284	2.545	2.772	2.974	3.156	3.320	3.470
.35	.435	.648	.819	.967	1.099	1.219	1.329	1.432	1.529	1.620	1.073	1.514	1.841	2.103	2.322	2.508	2.671	2.813	2.939	3.051
.40	.488	.721	.908	1.068	1.210	1.338	1.456	1.565	1.667	1.762	1.025	1.421	1.706	1.927	2.106	2.255	2.380	2.486	2.577	2.655
.45	.538	.790	.990	1.160	1.310	1.444	1.568	1.681	1.787	1.886	.978	1.331	1.575	1.757	1.900	2.012	2.103	2.176	2.235	2.282
.50	.586	.854	1.066	1.244	1.400	1.539	1.666	1.783	1.890	1.991	.931	1.243	1.448	1.594	1.701	1.781	1.840	1.884	1.914	1.933
.55	.631	.914	1.135	1.320	1.480	1.623	1.752	1.870	1.979	2.080	.886	1.157	1.325	1.437	1.512	1.562	1.593	1.609	1.614	1.609
.60	.674	.970	1.198	1.388	1.551	1.696	1.826	1.944	2.052	2.152	.841	1.073	1.206	1.286	1.332	1.355	1.360	1.352	1.334	1.309
.65	.715	1.022	1.256	1.448	1.613	1.758	1.888	2.005	2.112	2.211	.797	.992	1.093	1.143	1.162	1.160	1.143	1.114	1.077	1.033
.70	.754	1.069	1.308	1.502	1.668	1.812	1.940	2.055	2.160	2.256	.753	.914	.984	1.007	1.002	.978	.941	.894	.840	.781
.75	.791	1.113	1.354	1.549	1.714	1.856	1.982	2.095	2.197	2.289	.711	.838	.880	.878	.852	.808	.754	.692	.624	.553
.80	.825	1.153	1.396	1.590	1.753	1.893	2.016	2.125	2.223	2.311	.670	.765	.781	.757	.711	.651	.582	.507	.428	.347
.85	.858	1.190	1.433	1.625	1.785	1.922	2.041	2.146	2.240	2.324	.629	.695	.686	.643	.580	.505	.424	.339	.251	.163
.90	.888	1.223	1.464	1.654	1.811	1.944	2.058	2.159	2.248	2.328	.590	.628	.597	.536	.458	.372	.281	.187	.093	-.001
.95	.917	1.253	1.492	1.679	1.831	1.959	2.069	2.165	2.249	2.325	.552	.564	.513	.436	.346	.250	.151	.051	-.048	-.145
1.00	.943	1.279	1.516	1.698	1.846	1.969	2.074	2.164	2.244	2.314	.515	.502	.434	.343	.243	.138	.034	-.070	-.172	-.271
1.05	.968	1.303	1.536	1.713	1.855	1.973	2.073	2.158	2.233	2.298	.479	.444	.359	.257	.148	.038	-.071	-.178	-.281	-.380
1.10	.991	1.324	1.551	1.724	1.861	1.973	2.067	2.147	2.216	2.276	.444	.388	.290	.178	.062	-.053	-.164	-.272	-.375	-.473
1.15	1.012	1.342	1.565	1.731	1.862	1.968	2.056	2.131	2.195	2.251	.410	.336	.225	.105	-.016	-.133	-.246	-.354	-.456	-.552
1.20	1.032	1.357	1.574	1.735	1.859	1.960	2.042	2.112	2.171	2.221	.378	.286	.165	.038	-.086	-.205	-.318	-.424	-.524	-.617
1.25	1.050	1.370	1.581	1.735	1.853	1.948	2.025	2.089	2.143	2.189	.346	.239	.109	-.023	-.149	-.268	-.380	-.484	-.580	-.670
1.30	1.067	1.381	1.585	1.732	1.844	1.933	2.004	2.064	2.113	2.155	.316	.195	.057	-.078	-.205	-.323	-.433	-.533	-.627	-.712
1.35	1.082	1.390	1.587	1.727	1.833	1.915	1.982	2.036	2.081	2.118	.287	.154	.010	-.127	-.254	-.371	-.477	-.574	-.663	-.744
1.40	1.096	1.397	1.586	1.720	1.819	1.896	1.957	2.006	2.047	2.080	.260	.115	-.033	-.171	-.297	-.411	-.514	-.607	-.691	-.768
1.45	1.108	1.401	1.584	1.710	1.803	1.874	1.930	1.975	2.012	2.042	.233	.079	-.072	-.210	-.334	-.445	-.544	-.633	-.712	-.783
1.50	1.119	1.405	1.579	1.699	1.786	1.851	1.903	1.943	1.976	2.002	.208	.046	-.108	-.245	-.366	-.473	-.568	-.651	-.726	-.792
1.55	1.129	1.406	1.573	1.686	1.767	1.827	1.874	1.911	1.939	1.962	.184	.015	-.140	-.275	-.393	-.496	-.585	-.664	-.733	-.794
1.60	1.137	1.406	1.565	1.671	1.746	1.802	1.844	1.877	1.902	1.923	.161	-.013	-.168	-.301	-.415	-.513	-.598	-.672	-.736	-.792
1.65	1.145	1.405	1.556	1.656	1.725	1.776	1.814	1.843	1.866	1.883	.139	-.039	-.193	-.323	-.433	-.526	-.606	-.674	-.733	-.784
1.70	1.151	1.402	1.546	1.639	1.703	1.749	1.784	1.809	1.829	1.844	.118	-.063	-.216	-.342	-.447	-.535	-.610	-.673	-.727	-.773
1.75	1.157	1.399	1.535	1.622	1.681	1.722	1.753	1.776	1.793	1.806	.099	-.085	-.235	-.357	-.458	-.541	-.610	-.668	-.717	-.759
1.80	1.161	1.394	1.523	1.603	1.658	1.695	1.723	1.743	1.757	1.768	.081	-.104	-.252	-.370	-.465	-.543	-.607	-.660	-.705	-.742
1.85	1.165	1.388	1.510	1.585	1.634	1.668	1.692	1.710	1.723	1.732	.064	-.122	-.266	-.379	-.469	-.542	-.601	-.649	-.690	-.723
1.90	1.168	1.382	1.496	1.565	1.611	1.641	1.663	1.678	1.689	1.696	.048	-.137	-.278	-.386	-.471	-.538	-.593	-.637	-.673	-.702
1.95	1.170	1.375	1.482	1.546	1.587	1.614	1.633	1.646	1.655	1.662	.033	-.151	-.287	-.390	-.470	-.533	-.582	-.622	-.654	-.680
2.00	1.171	1.367	1.467	1.526	1.564	1.588	1.604	1.616	1.623	1.628	.019	-.163	-.295	-.393	-.467	-.525	-.570	-.606	-.634	-.657
2.05	1.171	1.358	1.452	1.507	1.540	1.562	1.576	1.586	1.592	1.596	.006	-.174	-.301	-.393	-.463	-.516	-.556	-.588	-.613	-.633
2.10	1.171	1.349	1.437	1.487	1.517	1.537	1.548	1.557	1.562	1.565	-.006	-.183	-.305	-.392	-.456	-.505	-.542	-.570	-.592	-.609
2.15	1.171	1.340	1.422	1.468	1.495	1.512	1.522	1.529	1.533	1.535	-.017	-.190	-.307	-.389	-.449	-.493	-.526	-.551	-.570	-.585
2.20	1.170	1.330	1.407	1.448	1.473	1.487	1.496	1.502	1.505	1.506	-.027	-.196	-.308	-.385	-.440	-.480	-.510	-.532	-.548	-.561
2.25	1.168	1.320	1.391	1.429	1.451	1.464	1.471	1.476	1.478	1.479	-.036	-.201	-.307	-.379	-.430	-.466	-.493	-.512	-.526	-.537
2.30	1.166	1.310	1.376	1.410	1.430	1.441	1.447	1.450	1.452	1.453	-.045	-.205	-.306	-.373	-.419	-.452	-.475	-.492	-.504	-.513
2.35	1.164	1.300	1.361	1.392	1.409	1.418	1.424	1.426	1.428	1.428	-.052	-.208	-.303	-.365	-.408	-.437	-.458	-.472	-.483	-.490
2.40	1.161	1.289	1.346	1.374	1.389	1.397	1.401	1.403	1.404	1.404	-.059	-.209	-.299	-.357	-.396	-.422	-.440	-.453	-.461	-.467

TABLE II. - Concluded. VALUES OF P_1 AND P'_1

η	P_1	P_2	P_3	P_4	P_5	P_6	P_7	P_8	P_9	P_{10}	P'_1	P'_2	P'_3	P'_4	P'_5	P'_6	P'_7	P'_8	P'_9	P'_{10}
2.45	1.158	1.279	1.331	1.356	1.369	1.376	1.380	1.381	1.381	1.381	-0.065	-0.210	-0.295	-0.348	-0.383	-0.407	-0.422	-0.433	-0.440	-0.445
2.50	1.154	1.268	1.316	1.339	1.350	1.356	1.359	1.360	1.360	1.359	-.070	-.210	-.290	-.339	-.371	-.391	-.405	-.414	-.420	-.424
2.55	1.151	1.258	1.302	1.322	1.332	1.337	1.339	1.340	1.339	1.339	-.075	-.209	-.284	-.329	-.358	-.376	-.388	-.395	-.400	-.403
2.60	1.147	1.248	1.288	1.306	1.315	1.319	1.320	1.320	1.320	1.319	-.079	-.207	-.278	-.319	-.345	-.361	-.371	-.377	-.381	-.383
2.65	1.143	1.237	1.274	1.290	1.298	1.301	1.302	1.302	1.301	1.300	-.082	-.205	-.271	-.309	-.331	-.345	-.354	-.359	-.362	-.363
2.70	1.139	1.227	1.261	1.275	1.282	1.284	1.285	1.284	1.284	1.283	-.085	-.202	-.263	-.298	-.318	-.330	-.338	-.342	-.344	-.345
2.75	1.134	1.217	1.248	1.261	1.266	1.268	1.268	1.268	1.267	1.266	-.087	-.199	-.256	-.287	-.305	-.316	-.322	-.325	-.326	-.327
2.80	1.130	1.207	1.235	1.246	1.251	1.253	1.253	1.252	1.251	1.250	-.089	-.195	-.248	-.276	-.292	-.301	-.306	-.309	-.310	-.310
2.85	1.126	1.198	1.223	1.233	1.237	1.238	1.238	1.237	1.236	1.235	-.090	-.191	-.240	-.266	-.280	-.287	-.291	-.293	-.294	-.293
2.90	1.121	1.188	1.211	1.220	1.223	1.224	1.223	1.223	1.222	1.221	-.090	-.187	-.232	-.255	-.267	-.274	-.277	-.278	-.278	-.278
2.95	1.117	1.179	1.200	1.207	1.210	1.210	1.210	1.209	1.208	1.207	-.091	-.182	-.223	-.244	-.255	-.260	-.263	-.264	-.264	-.263
3.00	1.112	1.170	1.189	1.192	1.198	1.198	1.197	1.196	1.195	1.194	-.091	-.177	-.215	-.234	-.243	-.247	-.249	-.250	-.249	-.249
3.10	1.103	1.153	1.168	1.173	1.174	1.174	1.174	1.173	1.172	1.171	-.090	-.166	-.198	-.213	-.220	-.223	-.224	-.224	-.223	-.222
3.20	1.094	1.137	1.149	1.153	1.154	1.153	1.152	1.151	1.151	1.150	-.087	-.155	-.182	-.193	-.198	-.200	-.201	-.200	-.199	-.198
3.30	1.085	1.122	1.132	1.134	1.135	1.134	1.133	1.133	1.132	1.131	-.084	-.143	-.166	-.175	-.178	-.179	-.179	-.178	-.177	-.176
3.40	1.077	1.108	1.116	1.118	1.118	1.117	1.116	1.116	1.115	1.114	-.080	-.132	-.150	-.157	-.160	-.160	-.159	-.159	-.158	-.157
3.50	1.069	1.095	1.102	1.103	1.103	1.102	1.101	1.101	1.100	1.100	-.076	-.121	-.136	-.141	-.142	-.142	-.142	-.141	-.140	-.139
3.60	1.062	1.084	1.089	1.090	1.089	1.089	1.088	1.087	1.087	1.086	-.071	-.110	-.122	-.126	-.127	-.126	-.126	-.125	-.124	-.123
3.70	1.055	1.073	1.077	1.078	1.077	1.077	1.076	1.076	1.075	1.075	-.066	-.099	-.109	-.112	-.112	-.112	-.111	-.110	-.109	-.109
3.80	1.049	1.064	1.067	1.067	1.067	1.066	1.066	1.065	1.065	1.065	-.061	-.089	-.097	-.098	-.098	-.098	-.098	-.097	-.096	-.096
3.90	1.043	1.056	1.058	1.058	1.058	1.057	1.057	1.056	1.056	1.056	-.056	-.080	-.086	-.087	-.087	-.087	-.086	-.085	-.085	-.084
4.00	1.038	1.048	1.050	1.050	1.049	1.049	1.049	1.048	1.048	1.048	-.051	-.071	-.076	-.077	-.076	-.076	-.075	-.075	-.074	-.074
4.10	1.033	1.041	1.043	1.043	1.042	1.042	1.042	1.041	1.041	1.041	-.046	-.063	-.067	-.067	-.067	-.066	-.066	-.065	-.065	-.064
4.20	1.028	1.035	1.036	1.036	1.036	1.036	1.035	1.035	1.035	1.035	-.041	-.055	-.058	-.059	-.058	-.058	-.057	-.057	-.056	-.056
4.30	1.025	1.030	1.031	1.031	1.031	1.030	1.030	1.030	1.030	1.030	-.037	-.049	-.051	-.051	-.050	-.050	-.050	-.049	-.049	-.049
4.40	1.021	1.026	1.026	1.026	1.026	1.026	1.025	1.025	1.025	1.025	-.033	-.042	-.044	-.044	-.044	-.043	-.043	-.043	-.042	-.042
4.50	1.018	1.022	1.022	1.022	1.022	1.022	1.022	1.021	1.021	1.021	-.029	-.037	-.038	-.038	-.038	-.037	-.037	-.037	-.037	-.036
4.60	1.015	1.018	1.019	1.018	1.018	1.018	1.018	1.018	1.018	1.018	-.025	-.032	-.033	-.033	-.032	-.032	-.032	-.032	-.031	-.031
4.70	1.013	1.015	1.016	1.015	1.015	1.015	1.015	1.015	1.015	1.015	-.022	-.027	-.028	-.028	-.028	-.027	-.027	-.027	-.027	-.027
4.80	1.011	1.013	1.013	1.013	1.013	1.013	1.013	1.013	1.013	1.013	-.019	-.023	-.024	-.024	-.023	-.023	-.023	-.023	-.023	-.023
4.90	1.009	1.011	1.011	1.011	1.011	1.011	1.010	1.010	1.010	1.010	-.016	-.020	-.020	-.020	-.020	-.020	-.020	-.020	-.019	-.019
5.00	1.008	1.009	1.009	1.009	1.009	1.009	1.009	1.009	1.009	1.009	-.014	-.017	-.017	-.017	-.017	-.017	-.017	-.017	-.016	-.016
5.10	1.006	1.007	1.007	1.007	1.007	1.007	1.007	1.007	1.007	1.007	-.012	-.014	-.014	-.014	-.014	-.014	-.014	-.014	-.014	-.014
5.20	1.005	1.006	1.006	1.006	1.006	1.006	1.006	1.006	1.006	1.006	-.010	-.012	-.012	-.012	-.012	-.012	-.012	-.012	-.012	-.012
5.30	1.004	1.005	1.005	1.005	1.005	1.005	1.005	1.005	1.005	1.005	-.009	-.010	-.010	-.010	-.010	-.010	-.010	-.010	-.010	-.010
5.40	1.004	1.004	1.004	1.004	1.004	1.004	1.004	1.004	1.004	1.004	-.007	-.008	-.008	-.008	-.008	-.008	-.008	-.008	-.008	-.008
5.50	1.003	1.003	1.003	1.003	1.003	1.003	1.003	1.003	1.003	1.003	-.006	-.007	-.007	-.007	-.007	-.007	-.007	-.007	-.007	-.007
5.60	1.002	1.003	1.003	1.003	1.003	1.003	1.003	1.003	1.003	1.003	-.005	-.006	-.006	-.006	-.006	-.006	-.006	-.006	-.006	-.006
5.70	1.002	1.002	1.002	1.002	1.002	1.002	1.002	1.002	1.002	1.002	-.004	-.005	-.005	-.005	-.005	-.005	-.005	-.005	-.005	-.005
5.80	1.002	1.002	1.002	1.002	1.002	1.002	1.002	1.002	1.002	1.002	-.003	-.004	-.004	-.004	-.004	-.004	-.004	-.004	-.004	-.004
5.90	1.001	1.001	1.001	1.001	1.001	1.001	1.001	1.001	1.001	1.001	-.003	-.003	-.003	-.003	-.003	-.003	-.003	-.003	-.003	-.003
6.00	1.001	1.001	1.001	1.001	1.001	1.001	1.001	1.001	1.001	1.001	-.002	-.002	-.002	-.002	-.002	-.002	-.002	-.002	-.002	-.002
6.10	1.001	1.001	1.001	1.001	1.001	1.001	1.001	1.001	1.001	1.001	-.002	-.002	-.002	-.002	-.002	-.002	-.002	-.002	-.002	-.002
6.20	1.001	1.001	1.001	1.001	1.001	1.001	1.001	1.001	1.001	1.001	-.001	-.002	-.002	-.002	-.002	-.002	-.002	-.002	-.002	-.002
6.30	1.000	1.000	1.000	1.000	1.000	1.000	1.000	1.000	1.000	1.000	-.001	-.001	-.001	-.001	-.001	-.001	-.001	-.001	-.001	-.001
6.40											0	0	0	0	0	0	0	0	0	0
6.50																				
6.60																				
6.70																				

TABLE III. - VALUES OF J_i

η	J_1	J_2	J_3	J_4	J_5	J_6	J_7	J_8	J_9	J_{10}
0	4.270	6.617	8.607	10.390	12.032	13.569	15.023	16.410	17.741	19.024
.05	4.217	6.446	8.373	10.120	11.626	13.132	14.518	15.783	17.048	18.253
.10	4.125	6.323	8.160	9.786	11.292	12.677	13.972	15.206	16.381	17.525
.15	4.035	6.163	7.93	9.496	10.901	12.226	13.451	14.616	15.720	16.784
.20	3.975	6.023	7.710	9.200	10.541	11.775	12.945	14.044	15.058	16.052
.25	3.902	5.868	7.514	8.904	10.189	11.347	12.434	13.446	14.422	15.337
.30	3.825	5.723	7.269	8.614	9.809	10.914	11.928	12.882	13.775	14.628
.35	3.744	5.577	7.049	8.322	9.459	10.491	11.438	12.325	13.159	13.943
.40	3.673	5.431	6.839	8.045	9.114	10.078	10.967	11.788	12.556	13.272
.45	3.603	5.290	6.630	7.768	8.772	9.670	10.500	11.257	11.967	12.630
.50	3.533	5.149	6.427	7.500	8.440	9.278	10.044	10.750	11.395	12.004
.55	3.459	5.010	6.222	7.236	8.113	8.897	9.604	10.251	10.849	11.402
.60	3.388	4.876	6.022	6.977	7.796	8.525	9.178	9.772	10.314	10.817
.65	3.319	4.744	5.830	6.721	7.487	8.160	8.764	9.307	9.804	10.263
.70	3.252	4.610	5.641	6.477	7.193	7.814	8.366	8.862	9.315	9.729
.75	3.185	4.482	5.453	6.238	6.902	7.474	7.982	8.437	8.848	9.218
.80	3.117	4.356	5.274	6.006	6.622	7.151	7.616	8.028	8.398	8.730
.85	3.053	4.234	5.098	5.782	6.351	6.838	7.262	7.633	7.970	8.269
.90	2.986	4.113	4.923	5.562	6.090	6.538	6.921	7.261	7.560	7.829
.95	2.924	3.996	4.758	5.354	5.839	6.247	6.598	6.904	7.172	7.414
1.00	2.859	3.878	4.597	5.149	5.598	5.970	6.289	6.562	6.804	7.017
1.05	2.798	3.767	4.412	4.952	5.363	5.704	5.993	6.239	6.456	6.644
1.10	2.738	3.658	4.285	4.763	5.142	5.451	5.711	5.932	6.122	6.288
1.15	2.678	3.551	4.141	4.580	4.927	5.208	5.440	5.639	5.808	5.956
1.20	2.616	3.440	3.990	4.398	4.712	4.968	5.176	5.354	5.503	5.630
1.25	2.564	3.345	3.860	4.236	4.524	4.756	4.944	5.100	5.232	5.345
1.30	2.509	3.248	3.727	4.073	4.336	4.546	4.713	4.854	4.969	5.068
1.35	2.454	3.153	3.600	3.918	4.158	4.344	4.496	4.619	4.721	4.805
1.40	2.402	3.062	3.476	3.770	3.987	4.155	4.289	4.396	4.486	4.559
1.45	2.350	2.971	3.359	3.626	3.823	3.974	4.092	4.188	4.266	4.330
1.50	2.299	2.886	3.244	3.490	3.669	3.802	3.909	3.992	4.059	4.113
1.55	2.250	2.802	3.134	3.360	3.521	3.640	3.734	3.808	3.864	3.909
1.60	2.200	2.721	3.028	3.234	3.379	3.487	3.568	3.632	3.680	3.721
1.65	2.154	2.643	2.927	3.116	3.245	3.341	3.413	3.467	3.511	3.543
1.70	2.108	2.567	2.831	3.001	3.118	3.203	3.267	3.313	3.349	3.377
1.75	2.064	2.496	2.738	2.894	2.999	3.072	3.127	3.168	3.199	3.222
1.80	2.020	2.425	2.650	2.789	2.885	2.949	2.998	3.032	3.057	3.076
1.85	1.978	2.357	2.564	2.692	2.775	2.833	2.874	2.904	2.926	2.941
1.90	1.938	2.293	2.482	2.597	2.673	2.723	2.759	2.784	2.802	2.814
1.95	1.898	2.231	2.404	2.508	2.575	2.619	2.650	2.671	2.685	2.696
2.00	1.859	2.171	2.329	2.423	2.483	2.522	2.547	2.566	2.577	2.585
2.05	1.821	2.112	2.258	2.344	2.395	2.409	2.451	2.466	2.476	2.482
2.10	1.785	2.056	2.190	2.267	2.312	2.343	2.360	2.373	2.381	2.386
2.15	1.751	2.004	2.126	2.195	2.235	2.261	2.276	2.286	2.292	2.295
2.20	1.717	1.952	2.065	2.125	2.162	2.183	2.196	2.205	2.209	2.210
2.25	1.684	1.903	2.005	2.060	2.092	2.111	2.121	2.128	2.131	2.132
2.30	1.652	1.856	1.950	1.998	2.026	2.042	2.050	2.055	2.058	2.059
2.35	1.622	1.812	1.897	1.940	1.964	1.976	1.985	1.988	1.990	1.990

TABLE III. - Concluded. VALUES OF J_i

η	J_1	J_2	J_3	J_4	J_5	J_6	J_7	J_8	J_9	J_{10}
2.40	1.593	1.768	1.846	1.885	1.905	1.916	1.922	1.925	1.926	1.926
2.45	1.564	1.728	1.798	1.832	1.849	1.859	1.864	1.866	1.866	1.866
2.50	1.536	1.688	1.752	1.782	1.797	1.805	1.808	1.809	1.809	1.808
2.55	1.510	1.651	1.709	1.735	1.748	1.754	1.757	1.758	1.757	1.757
2.60	1.485	1.616	1.667	1.691	1.702	1.708	1.709	1.709	1.709	1.708
2.65	1.460	1.580	1.628	1.648	1.658	1.662	1.664	1.664	1.662	1.661
2.70	1.437	1.548	1.591	1.609	1.618	1.620	1.621	1.620	1.620	1.619
2.75	1.414	1.517	1.556	1.572	1.578	1.581	1.581	1.581	1.579	1.578
2.80	1.392	1.487	1.522	1.535	1.542	1.544	1.544	1.543	1.542	1.540
2.85	1.372	1.460	1.490	1.503	1.508	1.509	1.509	1.508	1.506	1.505
2.90	1.352	1.432	1.460	1.471	1.475	1.476	1.475	1.475	1.473	1.472
2.95	1.333	1.407	1.432	1.440	1.444	1.444	1.444	1.443	1.442	1.440
3.00	1.314	1.383	1.405	1.412	1.416	1.416	1.415	1.414	1.412	1.411
3.10	1.280	1.338	1.356	1.361	1.362	1.362	1.362	1.361	1.360	1.359
3.20	1.249	1.208	1.311	1.316	1.317	1.316	1.315	1.314	1.314	1.313
3.30	1.220	1.261	1.273	1.275	1.276	1.275	1.274	1.274	1.273	1.272
3.40	1.194	1.229	1.238	1.240	1.240	1.239	1.238	1.238	1.236	1.235
3.50	1.171	1.199	1.207	1.208	1.208	1.207	1.206	1.206	1.205	1.205
3.60	1.150	1.174	1.179	1.180	1.179	1.179	1.178	1.177	1.177	1.176
3.70	1.131	1.150	1.155	1.156	1.155	1.155	1.154	1.154	1.153	1.153
3.80	1.115	1.131	1.134	1.134	1.134	1.133	1.133	1.132	1.132	1.132
3.90	1.099	1.113	1.115	1.115	1.115	1.114	1.114	1.113	1.113	1.113
4.00	1.086	1.097	1.099	1.099	1.098	1.098	1.098	1.097	1.097	1.097
4.10	1.074	1.083	1.085	1.085	1.084	1.084	1.084	1.083	1.083	1.083
4.20	1.063	1.070	1.071	1.071	1.071	1.071	1.070	1.070	1.070	1.070
4.30	1.055	1.060	1.061	1.061	1.061	1.060	1.060	1.060	1.060	1.060
4.40	1.046	1.051	1.051	1.051	1.051	1.051	1.050	1.050	1.050	1.050
4.50	1.039	1.043	1.043	1.043	1.043	1.043	1.043	1.042	1.042	1.042
4.60	1.033	1.036	1.037	1.036	1.036	1.036	1.036	1.036	1.036	1.036
4.70	1.028	1.030	1.031	1.030	1.030	1.030	1.030	1.030	1.030	1.030
4.80	1.024	1.026	1.026	1.026	1.026	1.026	1.026	1.026	1.026	1.026
4.90	1.019	1.021	1.021	1.021	1.021	1.021	1.020	1.020	1.020	1.020
5.00	1.016	1.018	1.018	1.018	1.018	1.018	1.018	1.018	1.018	1.018
5.10	1.013	1.014	1.014	1.014	1.014	1.014	1.014	1.014	1.014	1.014
5.20	1.011	1.012	1.012	1.012	1.012	1.012	1.012	1.012	1.012	1.012
5.30	1.009	1.010	1.010	1.010	1.010	1.010	1.010	1.010	1.010	1.010
5.40	1.007	1.008	1.008	1.008	1.008	1.008	1.008	1.008	1.008	1.008
5.50	1.006	1.006	1.006	1.006	1.006	1.006	1.006	1.006	1.006	1.006
5.60	1.005	1.005	1.005	1.005	1.005	1.005	1.005	1.005	1.005	1.005
5.70	1.004	1.004	1.004	1.004	1.004	1.004	1.004	1.004	1.004	1.004
5.80	1.003	1.003	1.003	1.003	1.003	1.003	1.003	1.003	1.003	1.003
5.90	1.002	1.002	1.002	1.002	1.002	1.002	1.002	1.002	1.002	1.002
6.00	1.002	1.002	1.002	1.002	1.002	1.002	1.002	1.002	1.002	1.002
6.10	1.002	1.002	1.002	1.002	1.002	1.002	1.002	1.002	1.002	1.002
6.20	1.001	1.001	1.001	1.001	1.001	1.001	1.001	1.001	1.001	1.001
6.30	1.001	1.001	1.001	1.001	1.001	1.001	1.001	1.001	1.001	1.001
6.40	1.000	1.000	1.000	1.000	1.000	1.000	1.000	1.000	1.000	1.000
6.50	1.000	1.000	1.000	1.000	1.000	1.000	1.000	1.000	1.000	1.000

TABLE IV. - VALUES OF H_i

η	H_1	H_2	H_3	H_4	H_5	H_6	H_7	H_8	H_9	H_{10}
0	0	0	0	0	0	0	0	0	0	0
.05	.053	.090	.122	.151	.176	.201	.224	.245	.266	.286
.10	.104	.177	.238	.292	.342	.388	.431	.472	.511	.549
.15	.151	.257	.345	.423	.493	.559	.620	.678	.733	.786
.20	.198	.334	.446	.545	.634	.716	.793	.866	.934	1.00
.25	.240	.404	.539	.656	.761	.858	.949	1.033	1.114	1.190
.30	.281	.470	.624	.758	.877	.987	1.088	1.183	1.273	1.357
.35	.319	.532	.703	.851	.983	1.103	1.213	1.316	1.413	1.504
.40	.355	.588	.775	.935	1.077	1.205	1.323	1.432	1.534	1.629
.45	.389	.641	.841	1.011	1.161	1.295	1.419	1.532	1.638	1.737
.50	.420	.688	.900	1.078	1.234	1.373	1.500	1.617	1.724	1.825
.55	.449	.732	.953	1.138	1.298	1.441	1.570	1.688	1.797	1.898
.60	.475	.770	.998	1.188	1.351	1.496	1.626	1.744	1.852	1.952
.65	.500	.807	1.041	1.233	1.398	1.543	1.673	1.790	1.897	1.996
.70	.522	.837	1.076	1.270	1.436	1.580	1.708	1.823	1.923	2.024
.75	.543	.865	1.106	1.301	1.466	1.608	1.734	1.847	1.949	2.041
.80	.560	.888	1.131	1.325	1.488	1.628	1.751	1.860	1.958	2.046
.85	.577	.909	1.152	1.344	1.504	1.641	1.760	1.865	1.959	2.043
.90	.591	.926	1.167	1.357	1.514	1.647	1.761	1.862	1.951	2.031
.95	.603	.939	1.178	1.365	1.517	1.645	1.755	1.851	1.935	2.011
1.00	.613	.949	1.186	1.368	1.516	1.639	1.744	1.834	1.914	1.984
1.05	.622	.957	1.190	1.367	1.509	1.627	1.727	1.812	1.887	1.952
1.10	.629	.962	1.189	1.362	1.499	1.611	1.705	1.785	1.854	1.914
1.15	.634	.964	1.187	1.353	1.484	1.590	1.678	1.753	1.817	1.873
1.20	.638	.963	1.180	1.341	1.465	1.566	1.648	1.718	1.780	1.827
1.25	.640	.960	1.171	1.325	1.443	1.538	1.615	1.679	1.733	1.779
1.30	.642	.956	1.160	1.307	1.419	1.508	1.579	1.639	1.688	1.730
1.35	.641	.949	1.146	1.286	1.392	1.474	1.541	1.595	1.640	1.677
1.40	.640	.941	1.130	1.264	1.363	1.440	1.501	1.550	1.591	1.624
1.45	.636	.929	1.112	1.238	1.331	1.402	1.458	1.503	1.540	1.570
1.50	.632	.918	1.092	1.212	1.299	1.364	1.416	1.456	1.489	1.515
1.55	.624	.901	1.068	1.181	1.262	1.322	1.369	1.406	1.434	1.457
1.60	.620	.889	1.048	1.154	1.229	1.285	1.327	1.360	1.385	1.406
1.65	.613	.873	1.024	1.124	1.193	1.244	1.282	1.311	1.334	1.351
1.70	.605	.856	1.000	1.093	1.157	1.203	1.238	1.263	1.283	1.298
1.75	.596	.838	.974	1.061	1.120	1.161	1.192	1.215	1.232	1.245
1.80	.586	.819	.948	1.028	1.083	1.120	1.148	1.168	1.182	1.193
1.85	.576	.799	.921	.996	1.045	1.079	1.103	1.121	1.134	1.143
1.90	.565	.779	.893	.962	1.008	1.038	1.060	1.075	1.086	1.093
1.95	.554	.759	.866	.930	.971	.998	1.017	1.030	1.039	1.046
2.00	.541	.737	.837	.896	.934	.958	.974	.986	.993	.998
2.05	.528	.715	.809	.864	.897	.919	.933	.943	.949	.953
2.10	.515	.693	.781	.831	.861	.881	.892	.901	.906	.909
2.15	.502	.671	.753	.799	.826	.843	.853	.860	.864	.866
2.20	.489	.649	.726	.767	.792	.806	.815	.821	.824	.825
2.25	.474	.626	.697	.735	.757	.770	.777	.782	.784	.785
2.30	.460	.604	.670	.704	.724	.735	.741	.744	.746	.747
2.35	.447	.583	.644	.675	.692	.701	.707	.709	.711	.711

TABLE IV. - Concluded. VALUES OF H_i

η	H_1	H_2	H_3	H_4	H_5	H_6	H_7	H_8	H_9	H_{10}
2.40	0.432	0.560	0.617	0.645	0.660	0.668	0.672	0.674	0.675	0.675
2.45	.418	.539	.591	.616	.629	.636	.640	.641	.641	.641
2.50	.403	.517	.575	.588	.599	.605	.608	.609	.609	.608
2.55	.389	.496	.540	.560	.570	.575	.577	.578	.577	.577
2.60	.375	.476	.516	.534	.534	.547	.548	.548	.548	.547
2.65	.360	.454	.491	.507	.515	.518	.519	.518	.518	.517
2.70	.346	.434	.468	.482	.489	.491	.492	.491	.491	.490
2.75	.332	.415	.446	.459	.464	.466	.466	.466	.465	.464
2.80	.318	.395	.423	.434	.439	.441	.441	.440	.439	.438
2.85	.305	.377	.402	.402	.416	.417	.417	.416	.415	.414
2.90	.292	.359	.382	.391	.394	.395	.394	.394	.393	.392
2.95	.279	.341	.362	.369	.372	.372	.372	.371	.370	.369
3.00	.266	.324	.343	.349	.352	.352	.351	.350	.349	.348
3.10	.241	.291	.306	.311	.312	.312	.312	.311	.310	.309
3.20	.218	.261	.273	.277	.278	.277	.276	.275	.275	.274
3.30	.196	.223	.243	.245	.246	.245	.224	.224	.243	.242
3.40	.175	.206	.214	.216	.216	.215	.214	.214	.213	.212
3.50	.156	.182	.189	.190	.190	.189	.188	.188	.187	.187
3.60	.139	.161	.166	.167	.166	.166	.165	.164	.164	.163
3.70	.122	.140	.144	.145	.144	.144	.143	.143	.142	.142
3.80	.108	.123	.126	.126	.126	.125	.125	.124	.124	.124
3.90	.094	.107	.109	.109	.109	.108	.108	.107	.107	.107
4.00	.082	.092	.094	.094	.093	.093	.093	.092	.092	.092
4.10	.071	.079	.081	.081	.080	.080	.080	.079	.079	.079
4.20	.061	.068	.069	.069	.069	.069	.068	.068	.068	.068
4.30	.053	.058	.059	.059	.059	.058	.058	.058	.058	.058
4.40	.045	.050	.050	.050	.050	.050	.049	.049	.049	.049
4.50	.038	.042	.042	.042	.042	.042	.042	.041	.041	.041
4.60	.033	.035	.036	.035	.035	.035	.035	.035	.035	.035
4.70	.029	.031	.032	.031	.031	.031	.031	.031	.031	.031
4.80	.023	.025	.025	.025	.025	.025	.025	.025	.025	.025
4.90	.019	.021	.021	.021	.021	.021	.021	.020	.020	.020
5.00	.016	.017	.017	.017	.017	.017	.017	.017	.017	.017
5.10	.012	.014	.014	.014	.014	.014	.014	.014	.014	.014
5.20	.011	.012	.012	.012	.012	.012	.012	.012	.012	.012
5.30	.009	.010	.010	.010	.010	.010	.010	.010	.010	.010
5.40	.008	.008	.008	.008	.008	.008	.008	.008	.008	.008
5.50	.006	.006	.006	.006	.006	.006	.006	.006	.006	.006
5.60	.005	.006	.006	.006	.006	.006	.006	.006	.006	.006
5.70	.004	.004	.004	.004	.004	.004	.004	.004	.004	.004
5.80	.004	.004	.004	.004	.004	.004	.004	.004	.004	.004
5.90	.002	.002	.002	.002	.002	.002	.002	.002	.002	.002
6.00	.002	.002	.002	.002	.002	.002	.002	.002	.002	.002
6.10	.002	.002	.002	.002	.002	.002	.002	.002	.002	.002
6.20	.002	.002	.002	.002	.002	.002	.002	.002	.002	.002
6.30	0	0	0	0	0	0	0	0	0	0
6.40	0	0	0	0	0	0	0	0	0	0
6.50	0	0	0	0	0	0	0	0	0	0

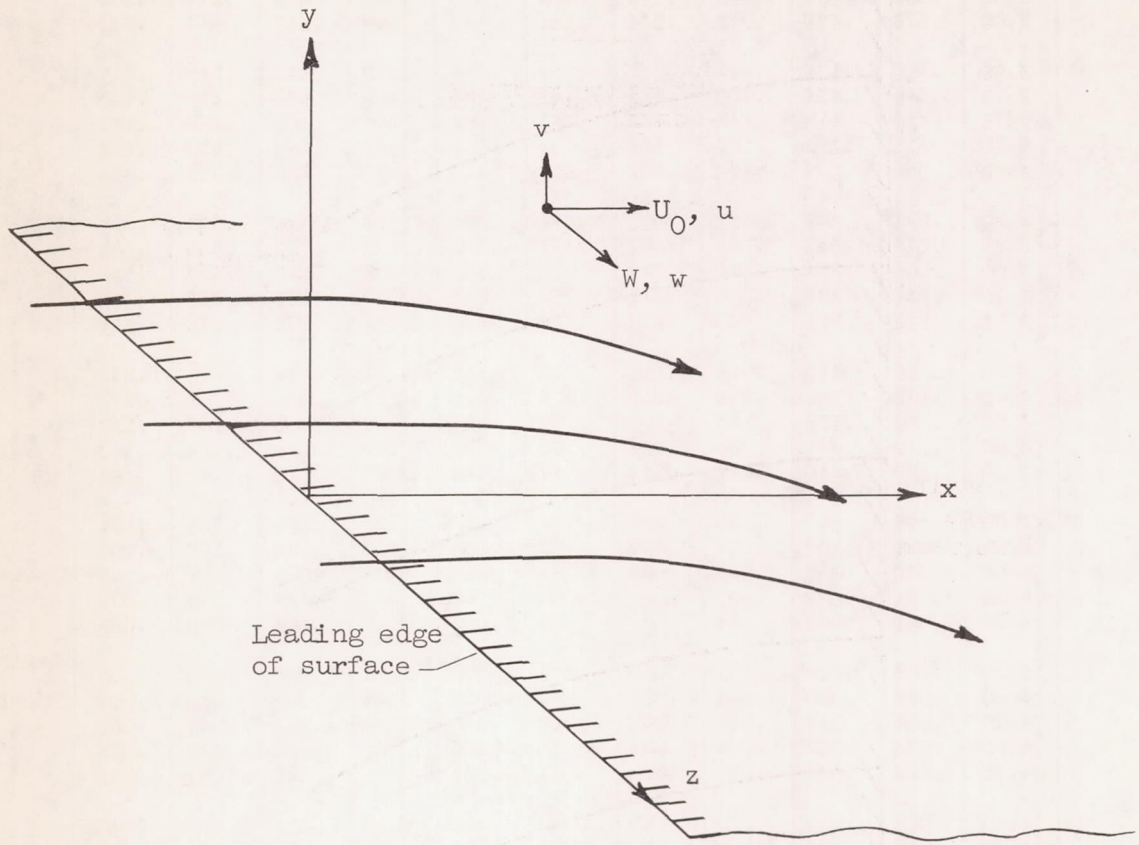

Figure 1. - Coordinate axes for flow over surface.

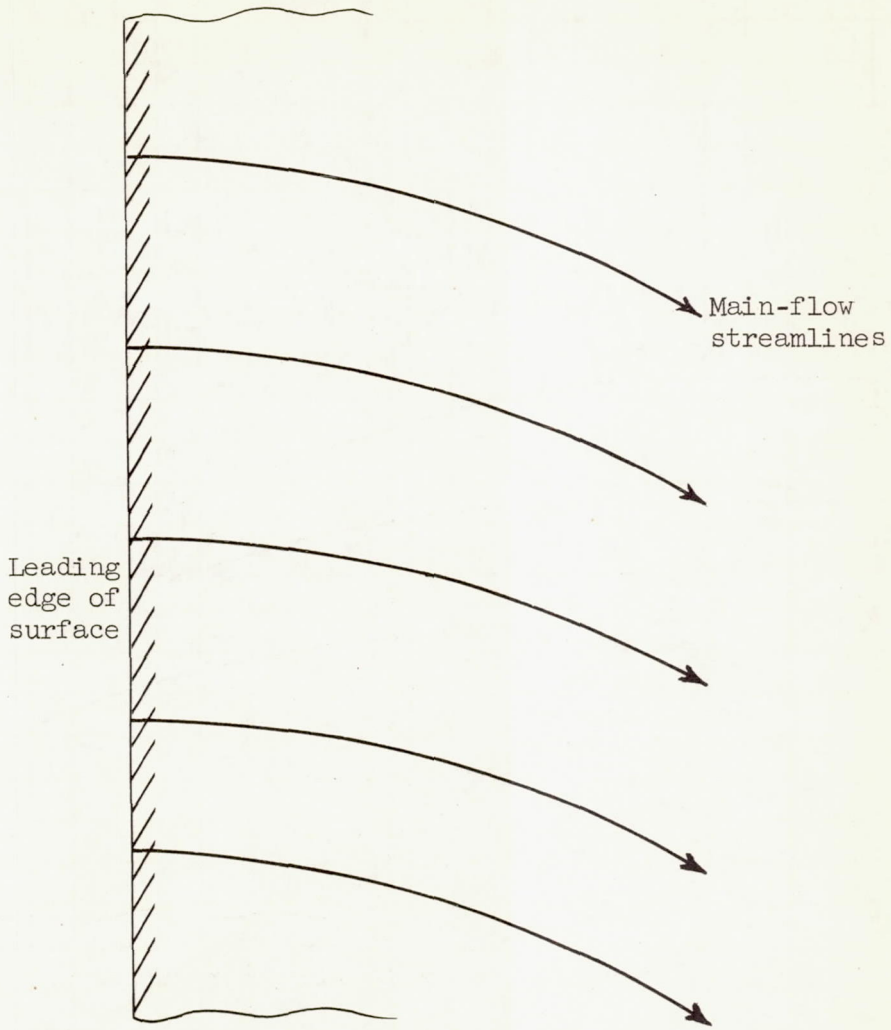

Figure 2. - Streamline pattern as system of translates.

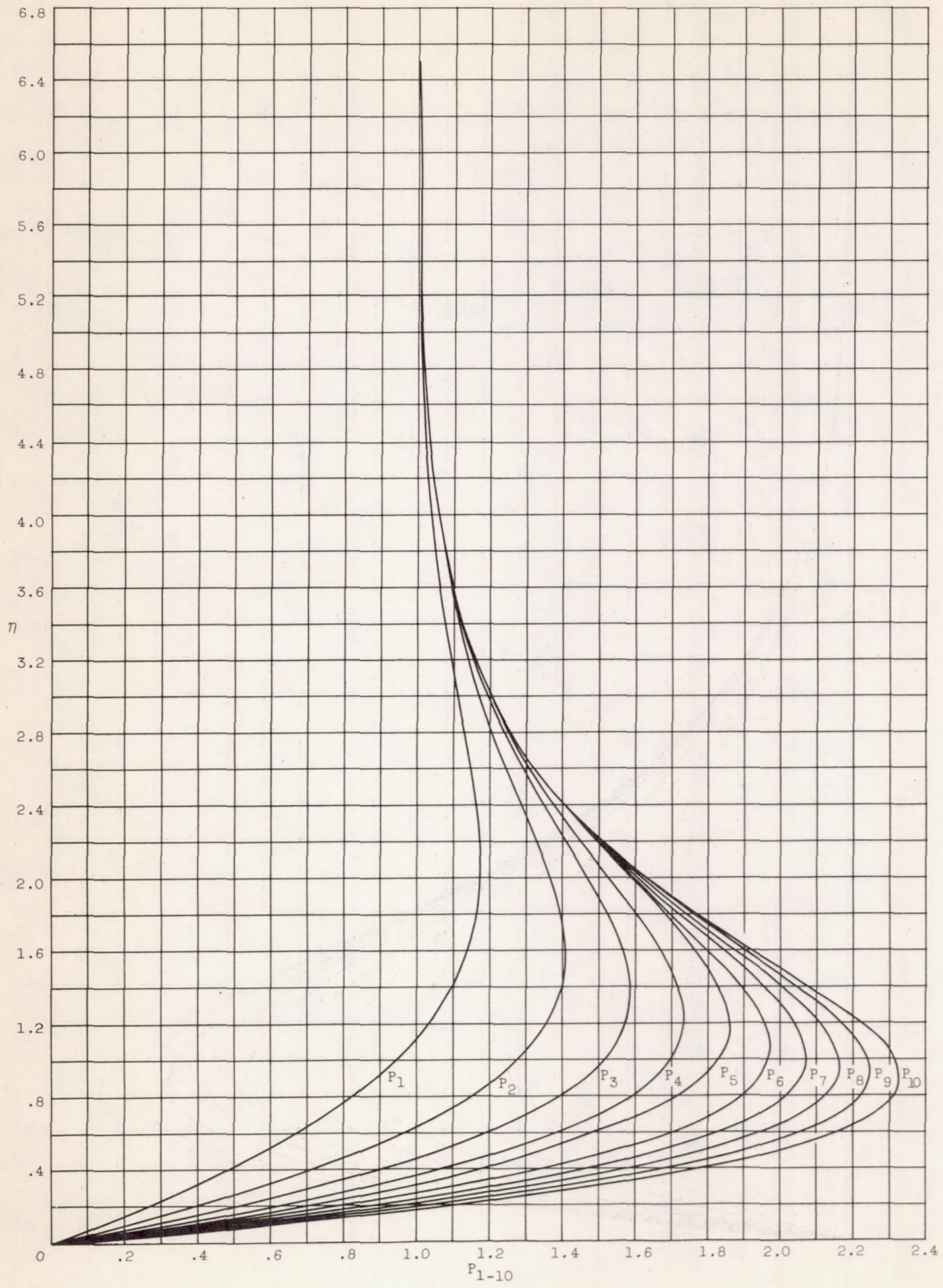

(a) $P_1(\eta)$.

Figure 3. - Functions of $P_1(\eta)$ and $H_1(\eta)$.

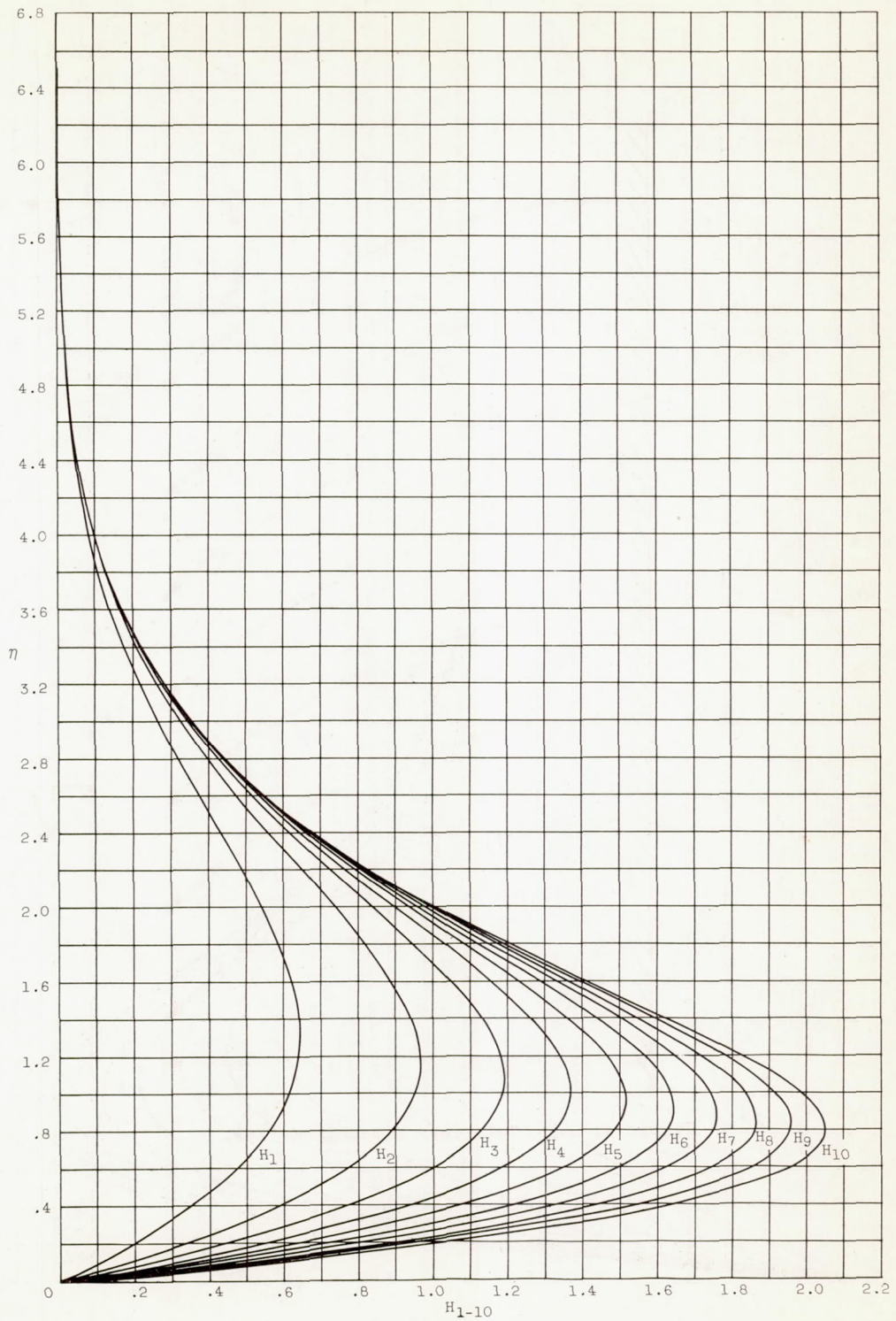

(b) $H_1(\eta)$.

Figure 3. - Concluded. Functions of $P_1(\eta)$ and $H_1(\eta)$.

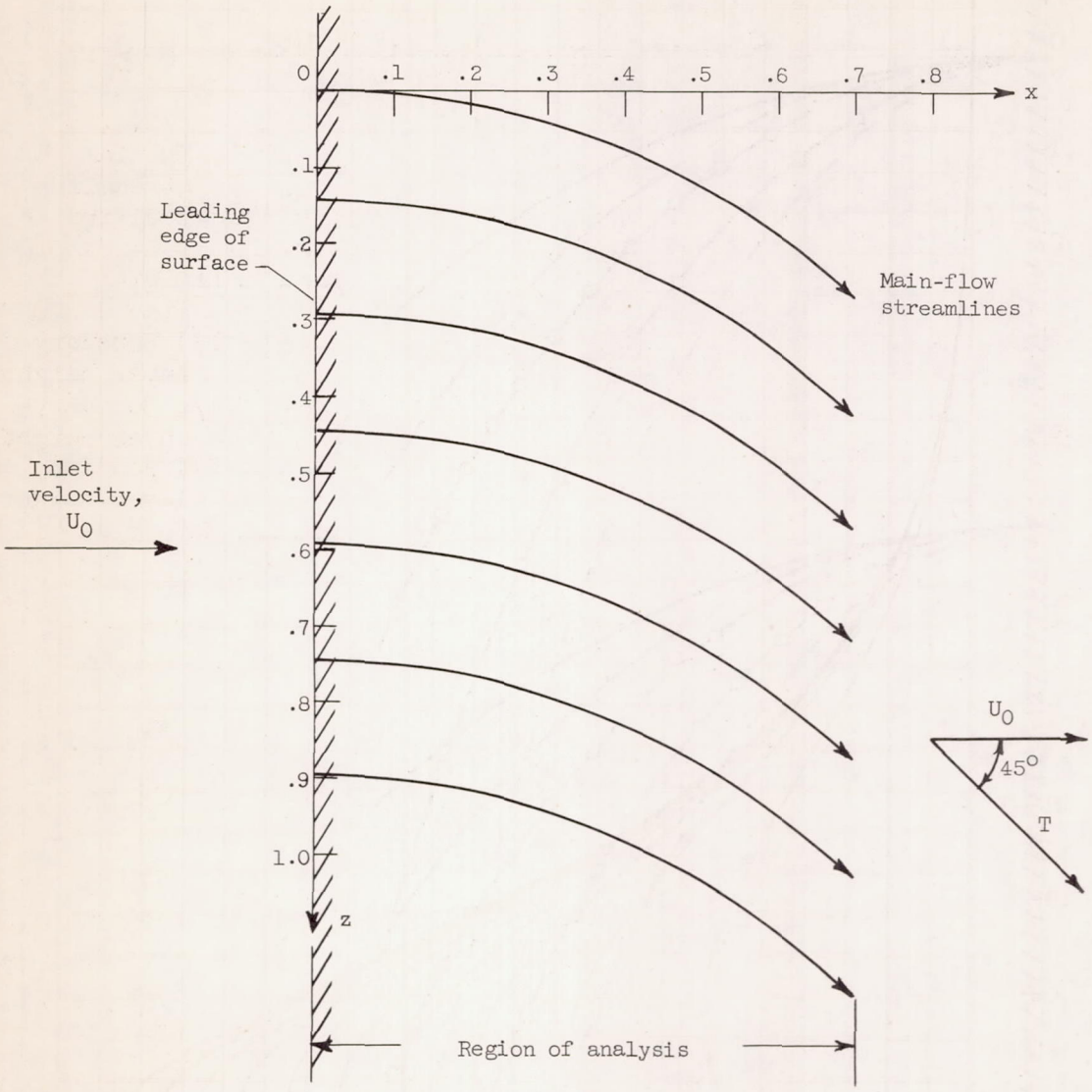

Figure 4. - Circular-arc streamline flow.

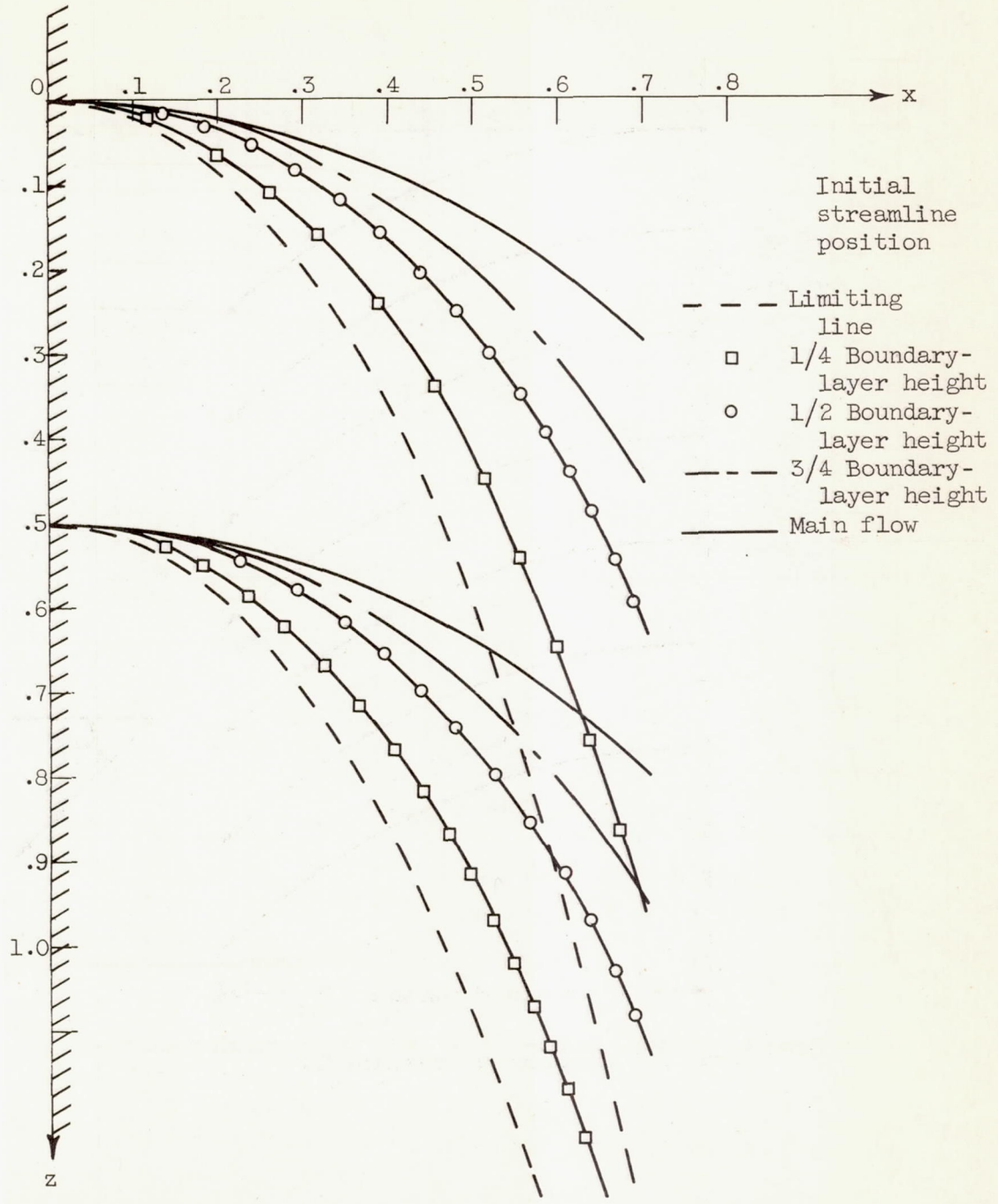

Figure 5. - Boundary-layer streamlines for circular-arc flow.

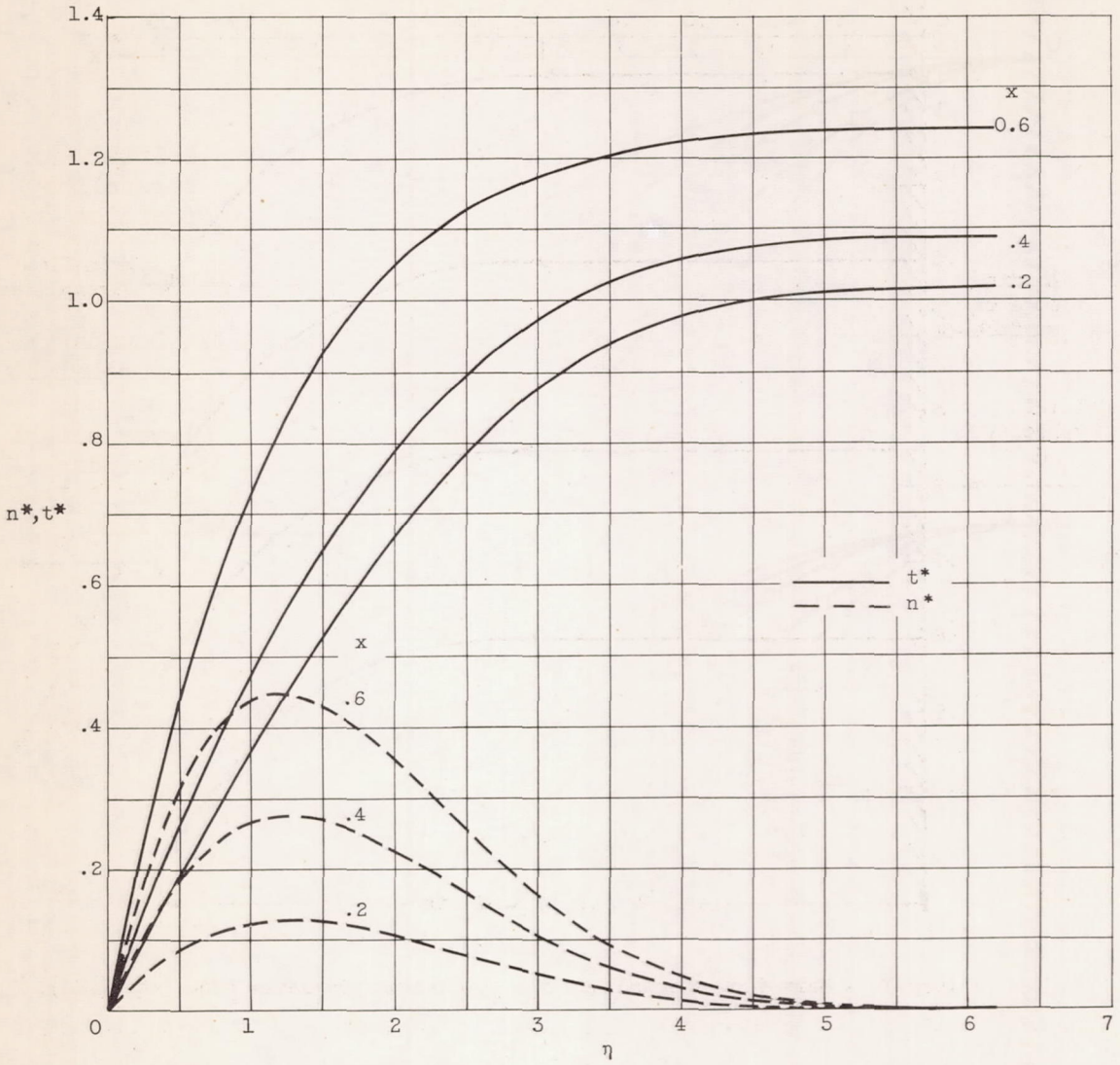

Figure 6. - Velocity profiles of n* and t* for circular-arc flow.

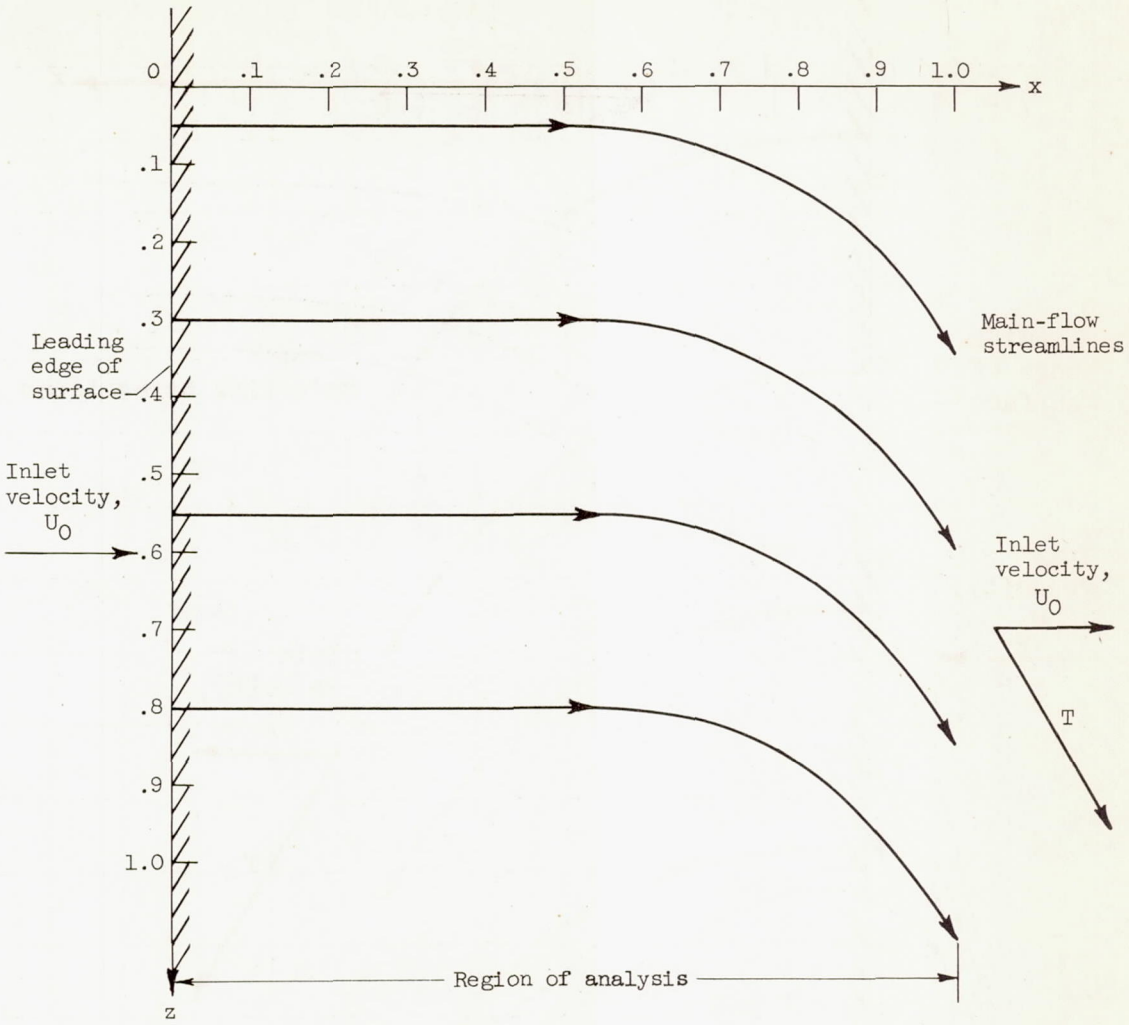

Figure 7. - Main-flow streamlines for thick-boundary-layer flow (eq. (26)).

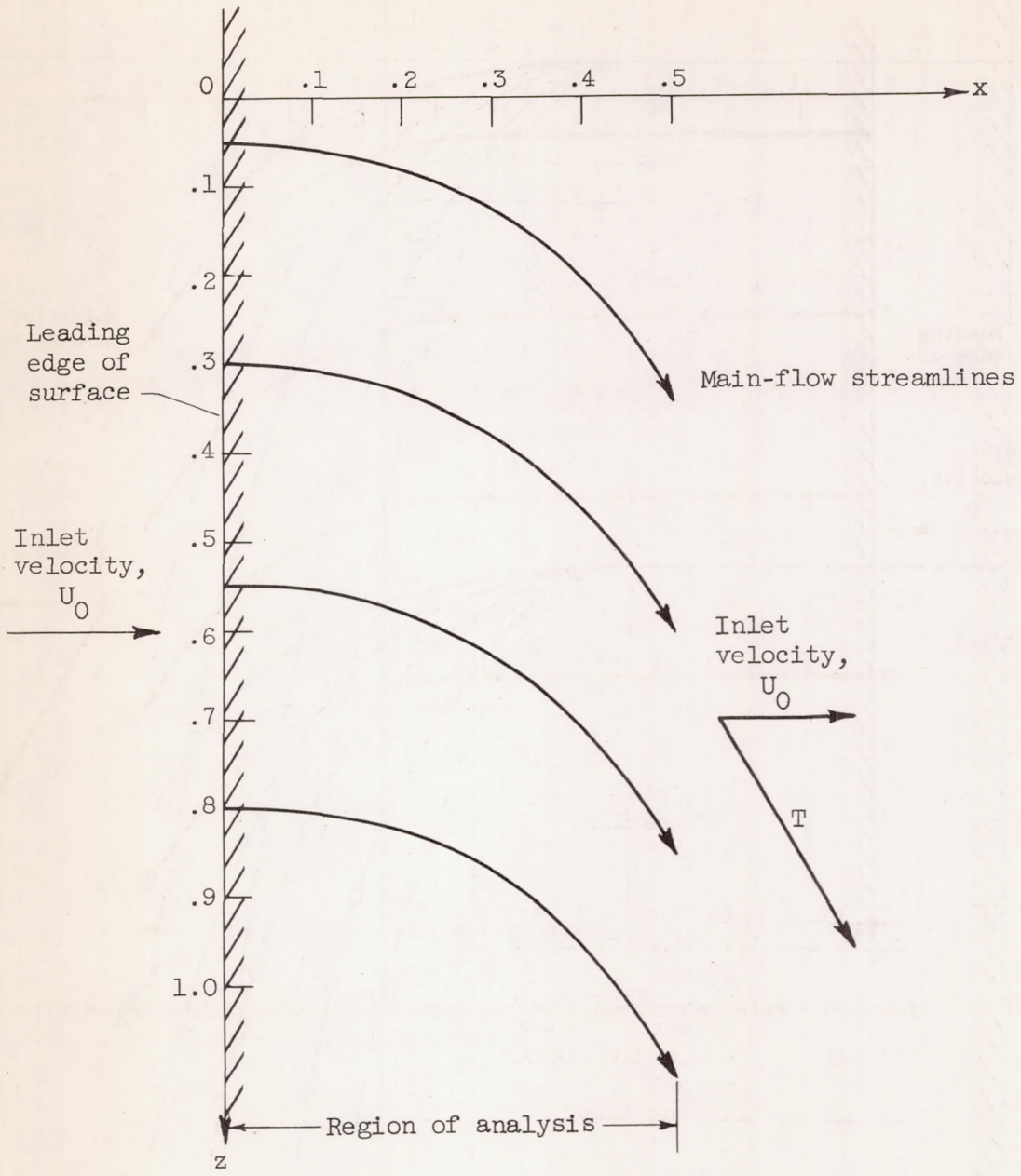

Figure 8. - Main-flow streamlines for thin-boundary-layer flow (eq. (27)).

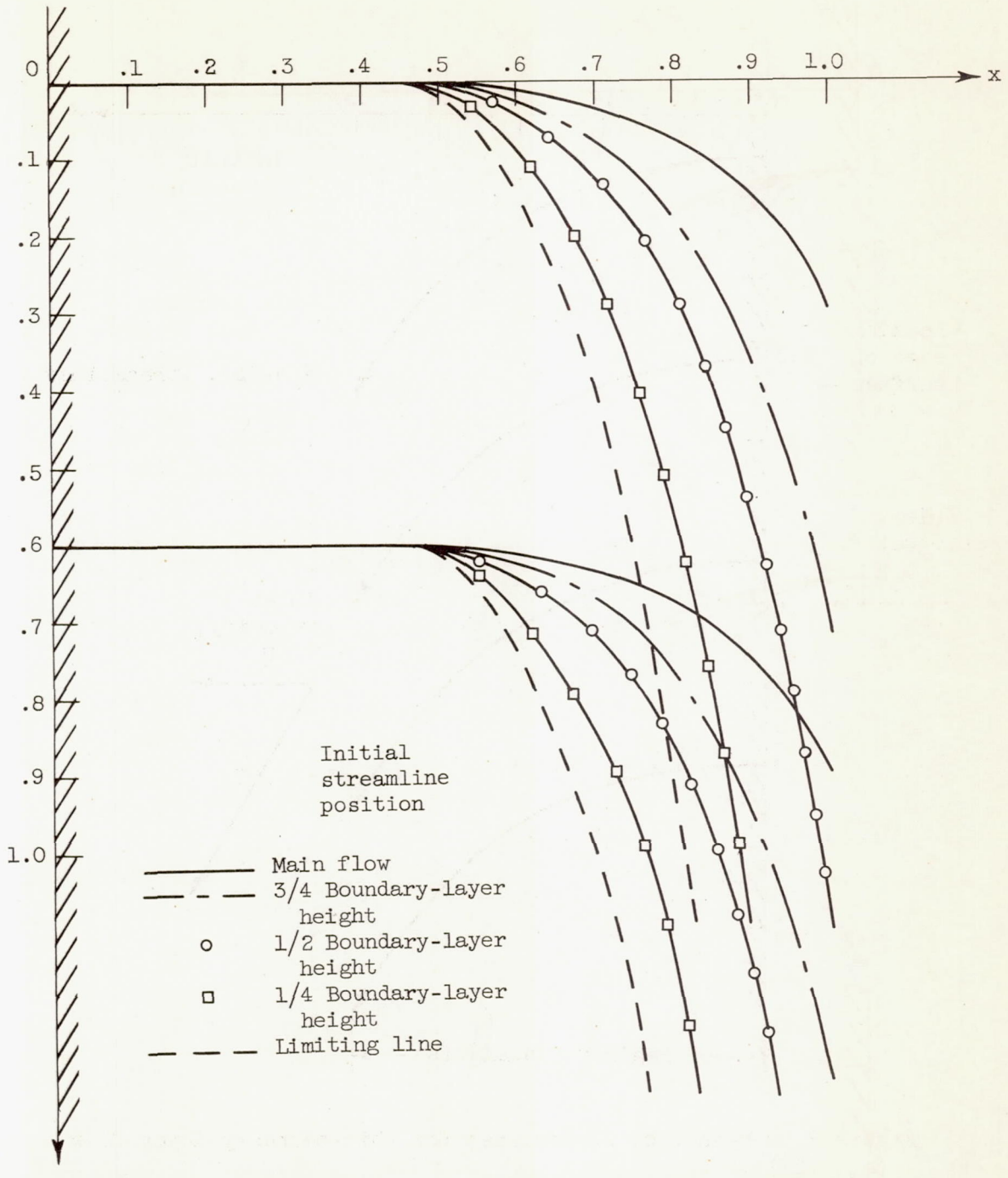

Figure 9. - Boundary-layer streamlines for thick-boundary-layer flow (eq. (26)).

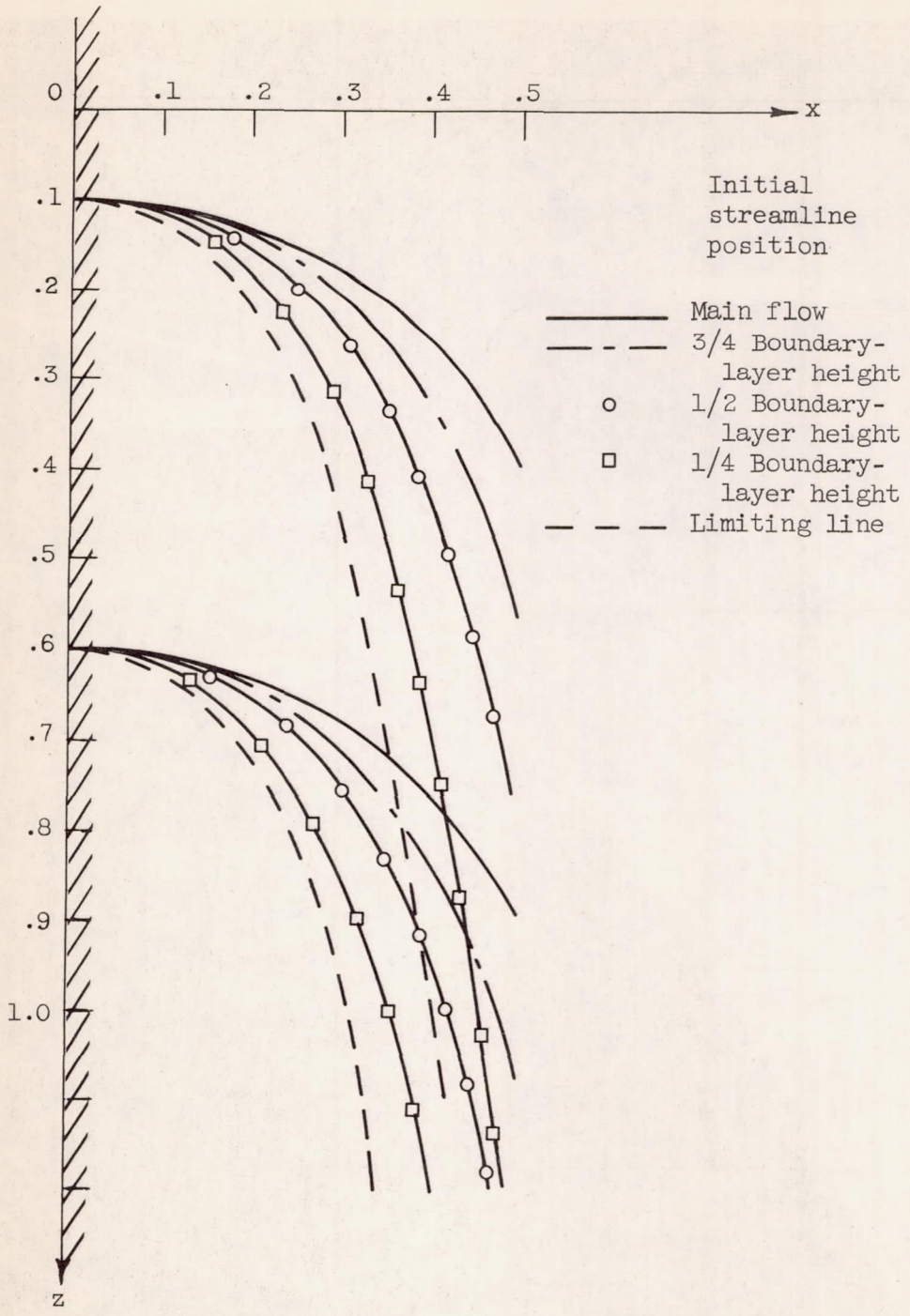

Figure 10. - Boundary-layer streamlines for thin-boundary-layer flow (eq. (27)).

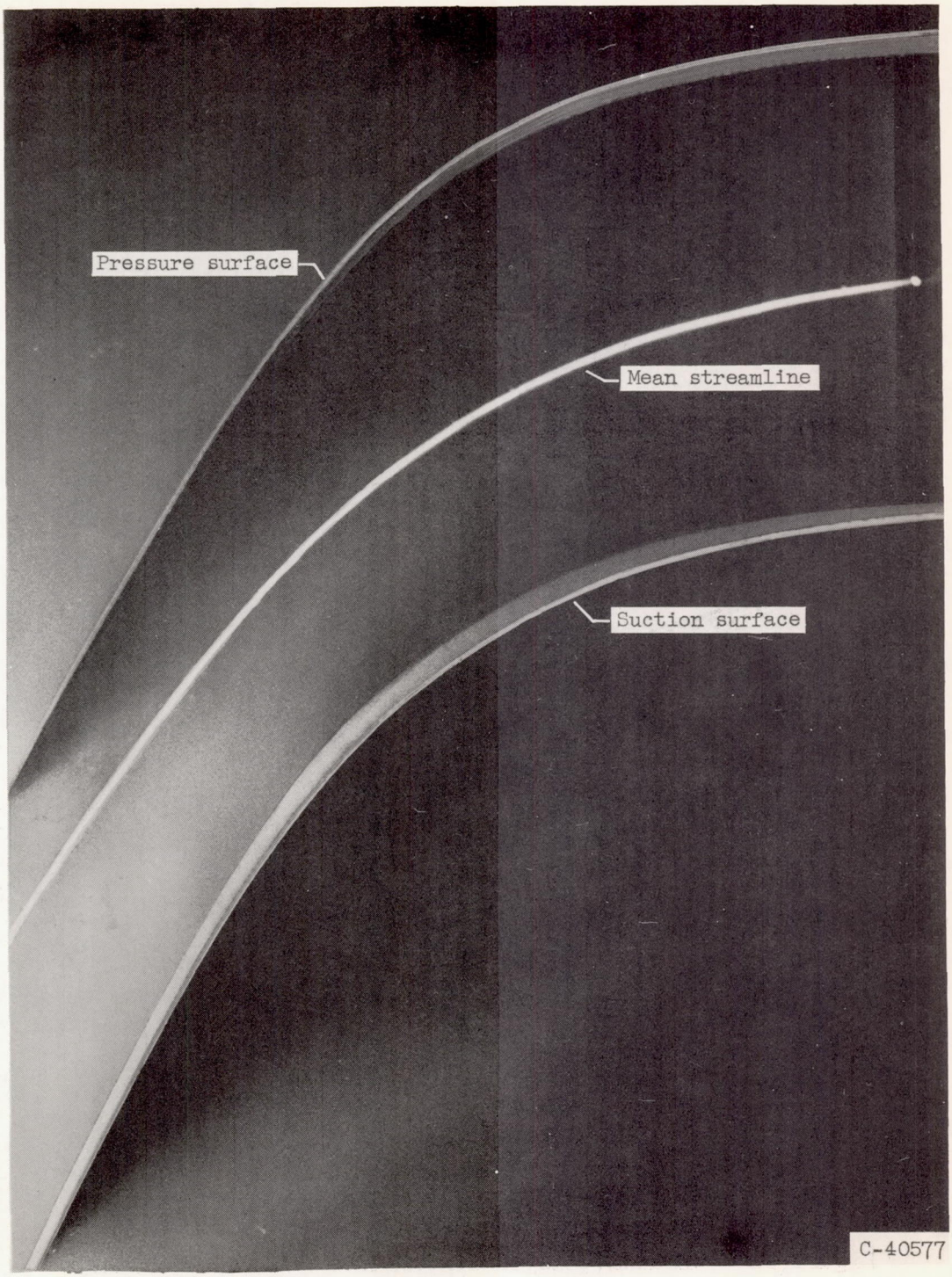

Figure 11. - Smoke-flow visualization of main streamline in 60°-turning rectangular bend.

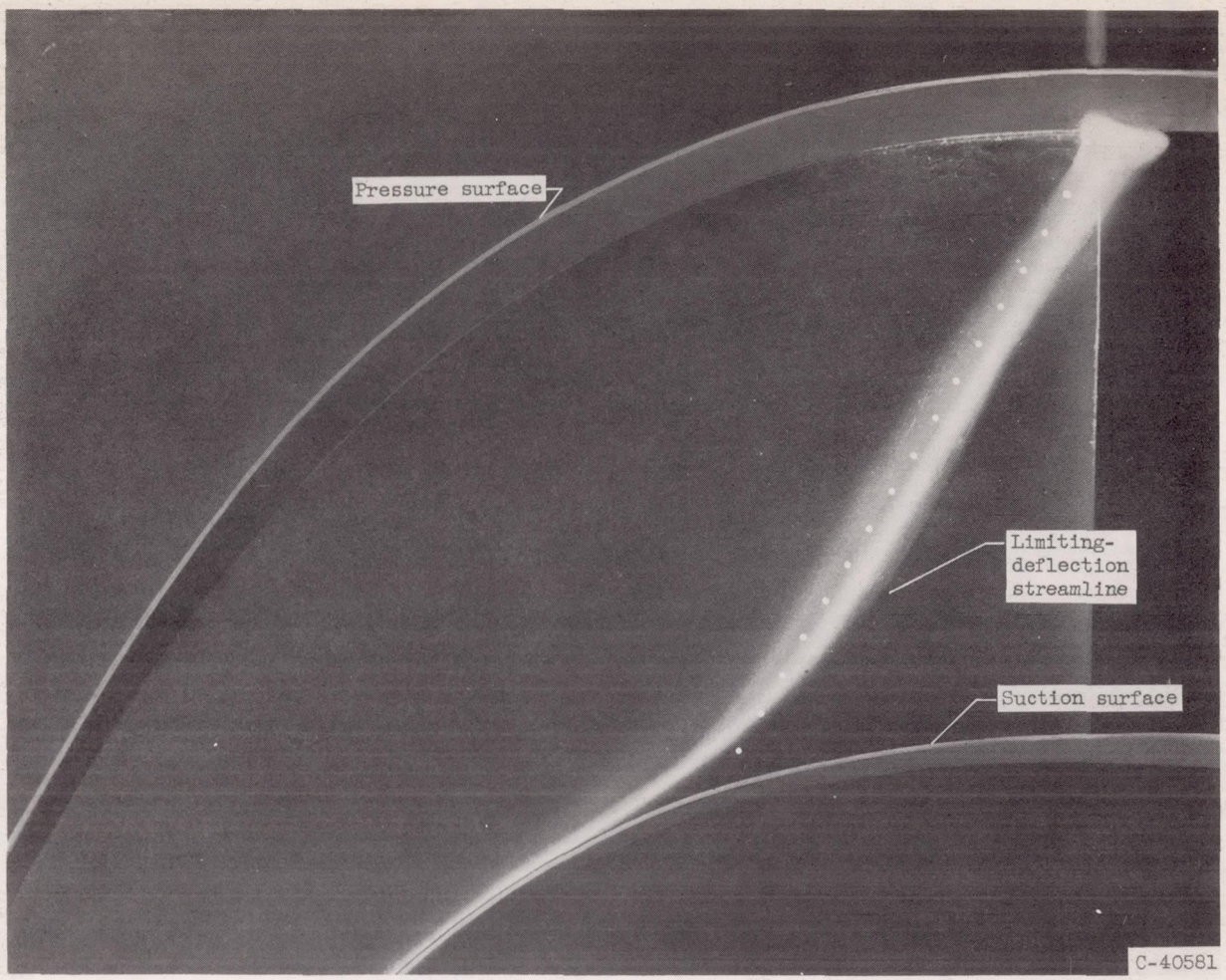

(a) Thick-boundary-layer limiting deflection.

Figure 12. - Smoke-flow visualization of limiting (η = 0) cross-channel deflection of boundary layer. Theoretical predictions shown as dotted lines.

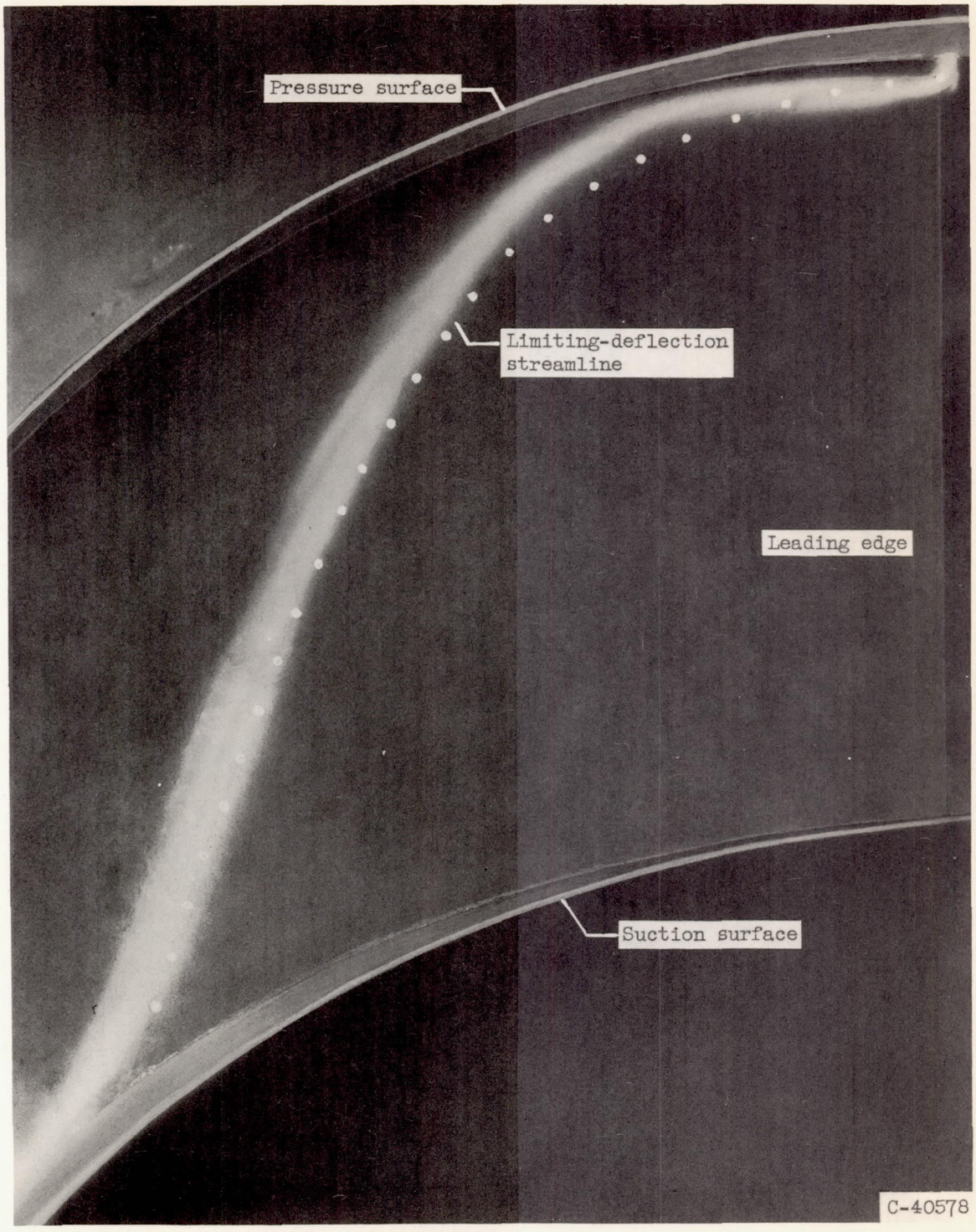

(b) Thin-boundary-layer limiting deflection.

Figure 12. - Concluded. Smoke-flow visualization of limiting (η = 0) cross-channel deflection of boundary layer. Theoretical predictions shown as dotted lines.

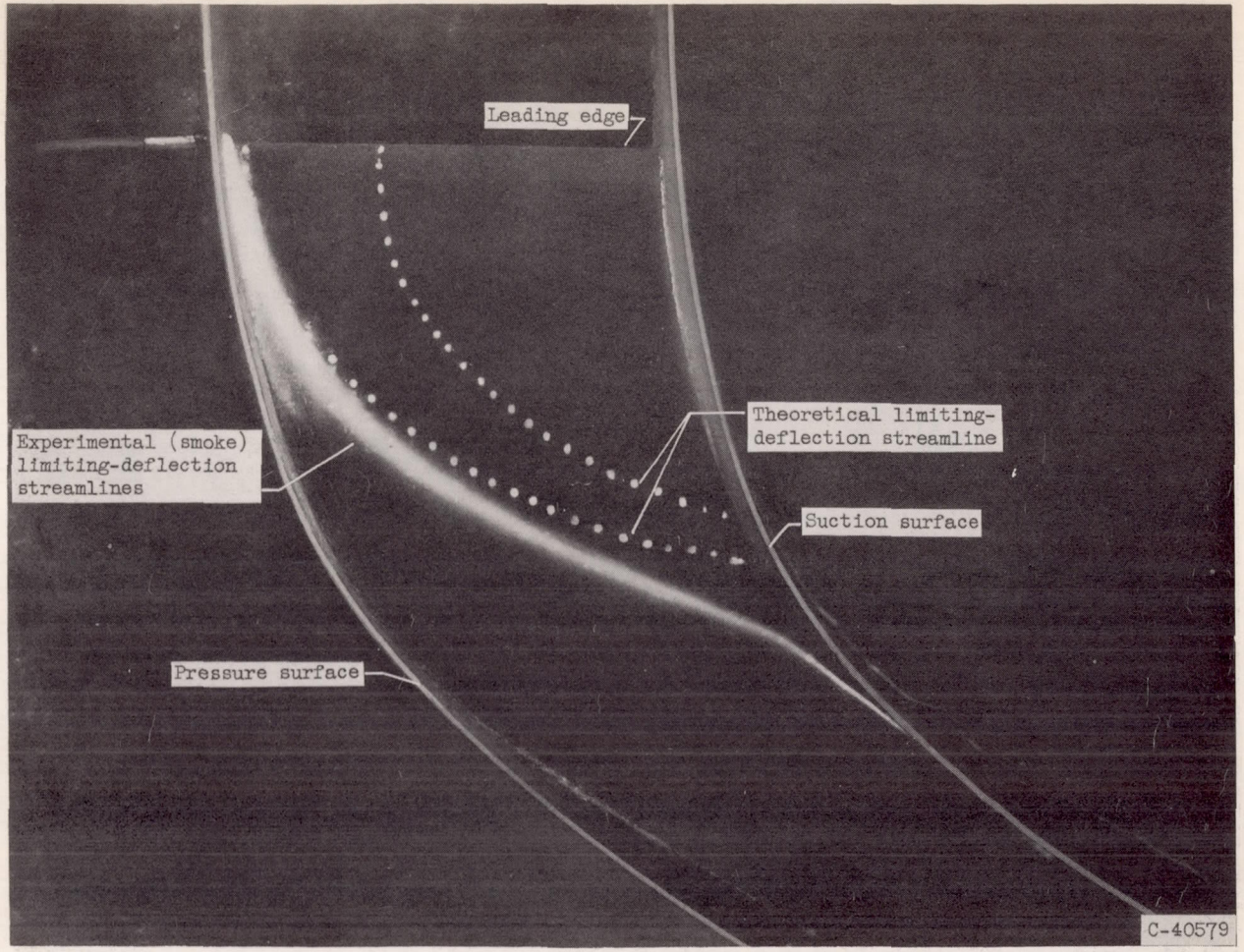

(a) Overhead view.

Figure 13. - Smoke-flow visualization of limiting deflection of cross-channel thin-boundary-layer flow.

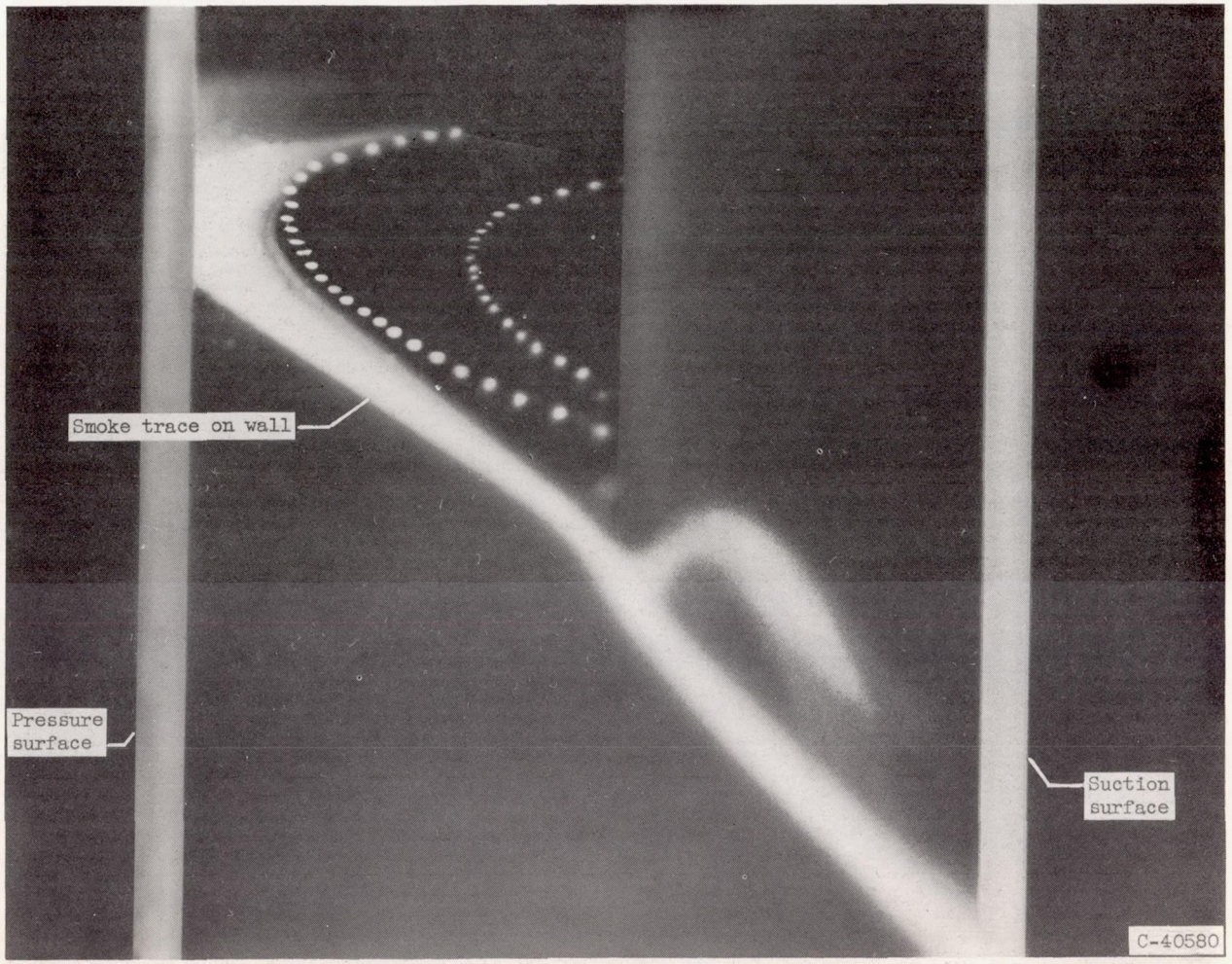

(b) Downstream view of boundary-layer streamline near pressure surface at inlet.

Figure 13. - Continued. Smoke-flow visualization of limiting deflection of cross-channel thin-boundary-layer flow.

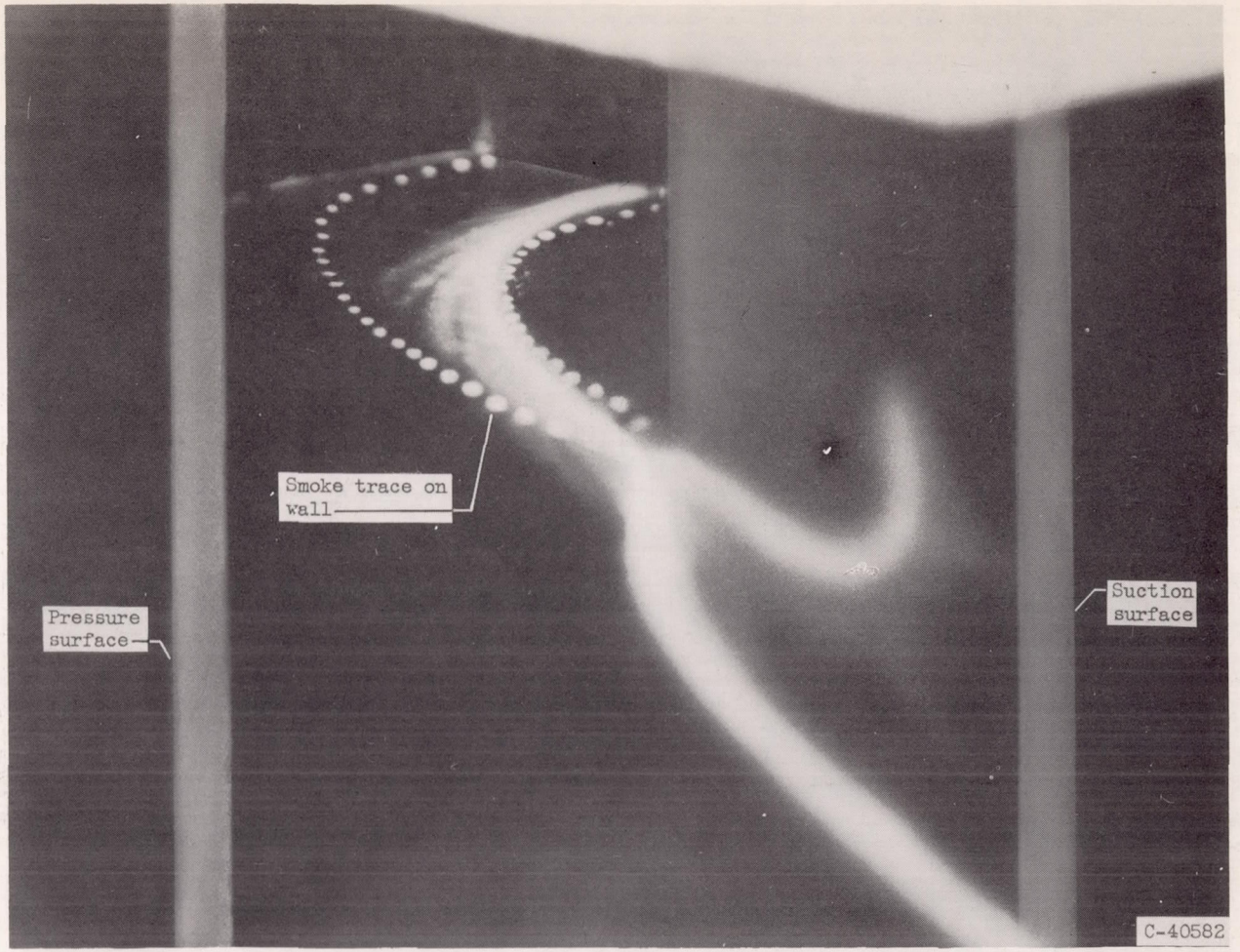

(c) Downstream view of boundary-layer streamline near midchannel at inlet.

Figure 13. - Concluded. Smoke-flow visualization of limiting deflection of cross-channel thin-boundary-layer flow.

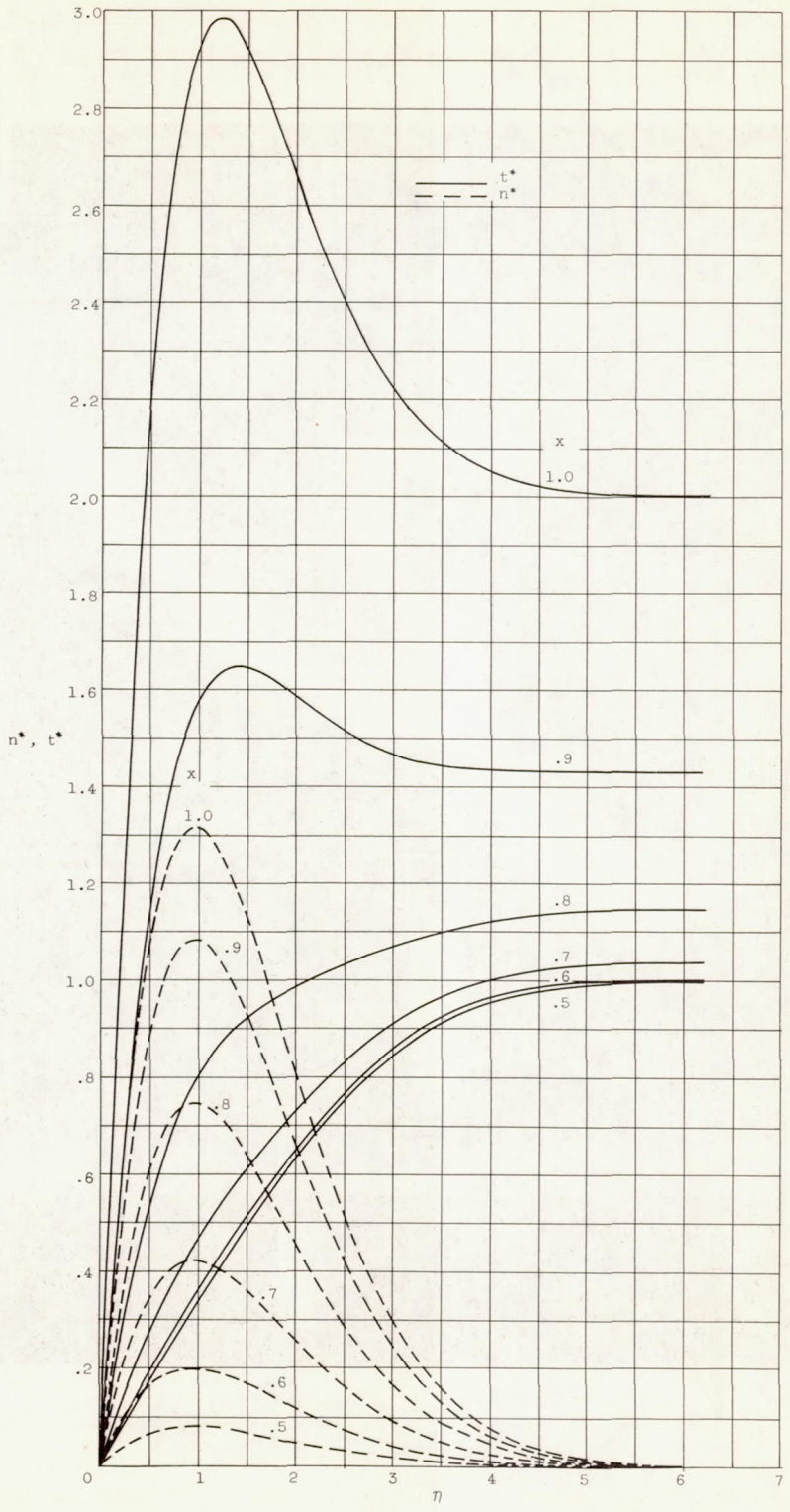

Figure 14. - Velocity profiles of n* and t* for thick-boundary-layer flow (eq. (26)).

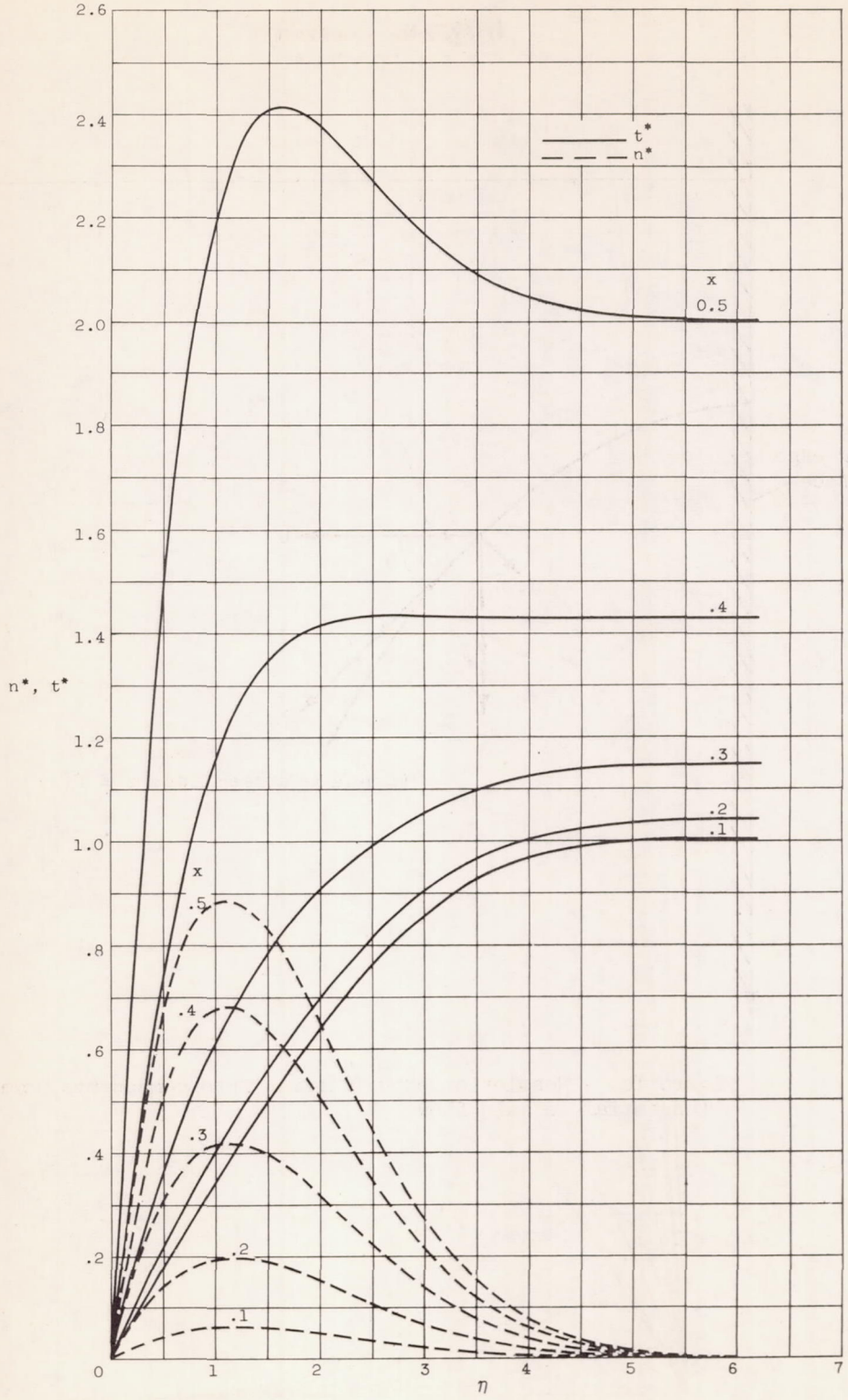

Figure 15. - Velocity profiles of n^* and t^* for thin-boundary-layer flow (eq. (27)).

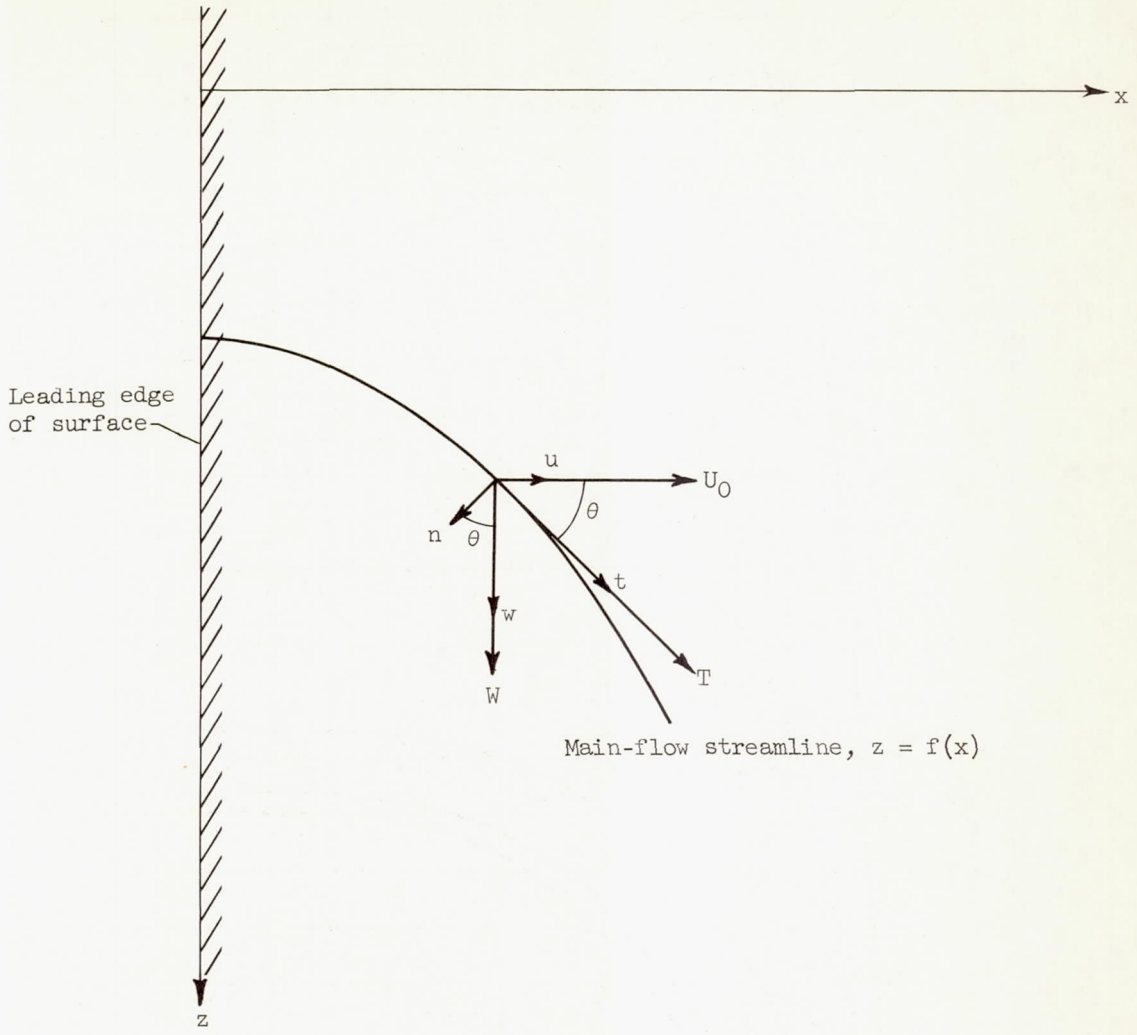

Figure 16. - Resolution of velocities into components normal and tangential to main flow.